Revisiting the influence of acid-base equilibrium and tautomerism on the free radical scavenging activities of curcumin derivatives in the physiological environment – A mechanistic and kinetic study

Dinh Hieu Truong,[1,2] Thi Tu Dinh,[3,4] Thi My Duyen Trinh,[5] Thi Hong Minh Pham,[3,4] Minh Quan Pham,[3,4] Urszula Gawlik-Dziki,[6] Duy Quang Dao,[1,2,*]

[1]*Institute of Research and Development, Duy Tan University, Da Nang 550000, Viet Nam*
[2]*School of Engineering and Technology, Duy Tan University, Da Nang 550000, Viet Nam*
[3]*Graduate University of Science and Technology, Vietnam Academy of Science and Technology, Hanoi, Viet Nam*
[4]*Institute of Natural Products Chemistry, Vietnam Academy of Science and Technology, Hanoi, Viet Nam*
[5]*Faculty of Pharmacy, Duy Tan University, Da Nang 550000, Viet Nam*
[6]*Department of Biochemistry and Food Chemistry, University of Life Sciences in Lublin, 8 Skromna St., 20-704 Lublin, Poland*

* Corresponding author: daoduyquang@duytan.edu.vn (D.Q.D.)

Abstract

Curcumin has been believed to have effective medicinal properties such as anti-cancer, anti-Alzheimer, anti-inflammatory, and antioxidant…, in which the free radical scavenging activities play a crucial role in its treating mechanisms. Although the antioxidant properties of curcumin and its derivatives have been widely studied in the literature, a systematical investigation of the thermodynamics and kinetics of the reaction towards hydroperoxide ($HOO^{\bullet}$), the standardized free radicals, has still been lacking. This work investigated the $HOO^{\bullet}$ radical scavenging activities of two curcumin derivatives, namely curcumin I (Cur-I) and curcumin III (Cur-III), in water and pentyl ethanoate (PEA) solutions using Density functional theory (DFT) approaches. The antioxidant properties of the neutral and anionic forms of two tautomers, including keto-enol and diketone of curcumin, were investigated *via* three common mechanisms, *i.e.*, hydrogen transfer (HT), radical adduct formation (RAF) and single electron transfer (SET). Intrinsic parameters, thermochemical parameters, and kinetics of the curcumin-HOO radical reactions were systematically characterized. As a result, the overall rate constant for the reaction in the water of Cur-I (9.36×10^7 M^{-1} s^{-1}) is about three times higher than the one of Cur-III (2.60×10^7 M^{-1} s^{-1}). Meanwhile, the ones in the PEA solvent are less significant, being 4.02×10^1 M^{-1} s^{-1} and 8.16×10^2 M^{-1} s^{-1}, respectively. Because of the dominant molar fraction of the keto-enol form compared to that of the diketone, the reaction rates were contributed mainly by the keto-enol form. Finally, the chemical nature of the HT processes was analyzed in detail, and it was found that all the most predominant HT reactions at the phenolic -OH groups (*i.e.*, O22H and O23H) occurred *via* the proton-coupled electron transfer (PCET) process.

Keywords: Curcumin I; curcumin III, antiradical, density functional theory, kinetics, QM-ORSA

Highlights

+ Thermodynamics and kinetics of HOO radical scavenging reactions of Cur-I and Cur-III were investigated in water and PEA solutions;

+ Influence of acid-base equilibrium on the reaction kinetics was performed;

+ Overall rate constants ($k_{Overall}$) in water are 9.36×10^7 and 2.60×10^7 M^{-1} s^{-1} for Cur-I and Cur-III;

+ $k_{Overall}$ in PEA are significantly less important, being of 4.02×10^1 and 8.06×10^2 M^{-1} s^{-1}, respectively;

+ Reaction of Cur-I with HOO radical is more dominant than Cur-III in water, but a reverse observation is found in PEA;

+ All the hydrogen transfer processes occur *via* the PCET mechanism.

1. Introduction

Curcumin, or 1,7-bis(4-hydroxy-3-methoxyphenyl)−1,6-heptadiene-3,5-dione, the most prevalent naturally occurring polyphenol is found in the roots of turmeric (*Curcuma longa* L.) and other Curcuma species. Curcuminoids, which comprise curcumin, desmethoxycurcumin, and bisdesmethoxycurcumin (Duvoix et al., 2005) [106]. Curcumin is an effective natural treatment that exhibits diverse medicinal activities, including anti-Alzheimer disease (Lim et al., 2001), anti-cancer (Mukhopadhyay et al., 2001), anti-inflammatory (Perrone et al., 2015), antioxidant (Masuda et al., 2001), antimicrobial (Negi et al., 1999), and anti-diabetic properties (Arun and Nalini, 2002).

Various works in the literature proved the neuroprotective influence of curcumin on the inhibition of Alzheimer's disease *via* different mechanisms (AD). Based on its activities of free radical scavenging and anti-inflammation, curcumin is also observed to prevent and diminish cellular inflammation-related neurodegeneration and aging processes(Moore et al., 2018; Santos-Parker et al., 2018) by binding to the amyloid β peptide (Aβ) central nervous systems. Lim *et al.* (2021) showed that low-dose curcumin treatment reduced the levels of amyloid-beta (Aβ) and plaque load in the brains of infected mice. Curcumin reduces the activity of γ-secretase by inhibiting the phosphorylation caused by the glycogen synthase kinase 3β (GSK-3β) of Presenilin 1 (PS1) (Lim et al., 2001). Curcumin compound directly influences the Aβ oligomers and fibers, depolymerizing and converting them into non-toxic aggregates while inhibiting Aβ monomer fibrillation (Kumaraswamy et al., 2013; Rao et al., 2015; Yang et al., 2005; Zhao et al., 2012). By using molecular dynamic (MD) simulations, Zhao et al. (2021) shed light on the depolymerization of Aβ oligomers and suggested that the π-stacking interaction between curcumin (keto ring and enol ring) and the aromatic residues of Aβ has diminished the β-sheet structure. Furthermore, the transition metals (*i.e.*, Zn, Fe, and Cu) in the rims and cores of senile plaques (SP) and the neuropil of the amygdala of AD patients were observed at high levels, which may enhance Aβ aggregation (Lovell et al., 1998). The ability of curcumin against Aβ (25–35)-induced toxicity in PC12 cells by chelating the redox-active metals, such as Fe and Cu, has been revealed as an indirect mechanism by which curcumin prevents Aβ aggregation (Park et al., 2008).

Curcumin also has several potential properties in cancer treatment. Gupta *et al*. indicated that head and neck squamous cell carcinoma (HNSCC), myeloma, and colorectal cancer can be partially treated by curcumin (Gupta et al., 2013). The anti-cancer capabilities of curcumin are based on its capacity to induce apoptosis and diminish tumor proliferation and invasion by inhibiting several cellular signaling pathways. The downstream gene products (c-myc, COX-2, NOS, Cyclin D1, TNF-α, interleukins, and MMP-9) and transcription factors are suppressed (Tomeh et al., 2019; Wilken et al., 2011). Curcumin combined with docetaxel commercial drug, which is used mainly for the treatment of various cancers, including breast,

lung, prostate, gastric, head, and neck, presents a positive effect on the PCa cell lines DU145 and PC3. The combination inhibited the proliferation and induced apoptosis higher than curcumin and docetaxel alone and modulates the expression of RTKs, PI3K, phospho-AKT, NF-kappa B, p53, and COX-2 (Singh, 2017).

Reactive free radicals are also believed to be one of the origins of inflammation, which is related to several chronic diseases (Lao et al., 2006; M.C. Recio et al., 2012; Panahi et al., 2016), such as Alzheimer's disease, Parkinson's disease, sclerosis, epilepsy, cerebral injury, cardiovascular disease, metabolic disorders, cancer, allergies, arthritis... Furthermore, inflammation may be one of the main reasons for developing age-related diseases (*i.e.*, cancer, infections, inflammatory diseases) (Cannizzo et al., 2011; Franceschi et al., 2000; Gruver et al., 2007). Curcumin is effective in treating chronic and acute inflammation (Mukhopadhyay et al., 1982). The anti-inflammatory characteristics of curcumin result from the prevention of neutrophil activity and the production of inflammatory prostaglandins from arachidonic acid (Mukhopadhyay et al., 1982).

As mentioned above, several diseases originate from the reactivities of free radicals and transition metal ions. Thus, the radical scavenging activities of curcumin have attracted several studies in the literature using experimental and computational approaches. Indeed, several experimental works show the efficient antioxidant capacity of curcumin and curcumin derivatives in preventing free radical damage in the human body(Ramirez-Boscá et al., 1995). The antioxidant properties of curcumin were reported to be comparable to those of vitamins C and E (Priyadarsini et al., 2003; Toda et al., 1985). Reactive nitrogen and oxygen species (RNS and ROS), as well as additional free radicals and ROS-producing enzymes like xanthine hydrogenase/oxidase and lipoxygenase/cyclooxygenase, can be eliminated and inactivated (Menon and Sudheer, 2007). The effects of curcumin on endothelial heme oxygenase-1 (HO-1) using cells from the bovine aortic endothelium were also investigated. The results showed that curcumin enhances cellular resistance to oxidative damage after 18 h of incubation (Motterlini et al., 2000).

Curcumin and its derivatives are also targeted objects of various Density functional theory (DFT) works in the literature (Alisi et al., 2020; Anjomshoa et al., 2017, 2016; Boulmokh et al., 2024; Galano et al., 2009; Hazarika and Kalita, 2021; Manzanilla and Robles, 2022; Vera-de La Garza et al., 2023). The reactivities of curcumin compounds have been predicted based on the evaluation of their electronic structures and the calculation of global quantum chemical indicators. Anjomshoa *et al*. used the DFT approach at the BMK/ 6-311+G(3df,2pd)//B3LYP/6-31G(2df,p) level of theory combined with the SMD solvation model to investigate the effect of solvent on tautomerism, acidity and radical stability of curcumin and some derivatives based on the thermodynamics parameters (Anjomshoa et al., 2016). Results showed that the keto-enol form is significantly more stable than the diketo form in all studied solvents (*i.e.*, water, DMSO, acetonitrile, ethanol, acetone…). Manzanilla and Robles investigated the antioxidant properties of

curcumin, caffeic acid phenethyl ester, and chicoric acid using DFT/M06-2X functional in conjunction with the 6–31+G* basis set based on the global chemical reactivity descriptors from conceptual DFT (Manzanilla and Robles, 2022). Some descriptors were calculated, such as electronegativity, vertical ionization energy, electron affinity, chemical hardness, and electrophilicity index. It is shown that diketone and keto-enol curcumins are found to be weaker electron donors and better electron acceptors; they are good anti-reductants according to the SET mechanism. Hazarika and Kalita (2021) also investigated the global quantum chemical parameters of diketone and keto-enol forms in the gas and DMSO solution using the B3LYP/6-311G(d,p) level (Hazarika and Kalita, 2021). Based on these indicators, the authors suggested that the enol form is more reactive than the keto one in both phases.

It is noteworthy that the approaches based on the electronic properties, the quantum chemical descriptors, or intrinsic thermochemical parameters (*i.e.*, bond dissociation enthalpy BDE, ionization potential IP, proton affinity PA…) only represent the chemical nature of the studied compounds, but do not consider the reactive radical species, or the environment conditions. To respond to this issue, various DFT works have focused on the reactivities of curcumin towards different free radicals using thermodynamics calculations or both thermodynamics and kinetics of reactions. For example, Sadatsharifi and Purgel (2021) evaluated the antiradical properties of alizarin and curcumin towards harmful small free radicals (*i.e.*, hydroxyl, peroxyl, and superoxide radicals) at the M062X/TZVP/SMD level of theory(Sadatsharifi and Purgel, 2021). All the possible pathways of the autoxidation through cyclic radical forms and the authors showed that the key intermediate is the epoxide form from which all cyclopentadione could be formed. Furthermore, hydroxyketocyclopentadione and hemiacetalcyclopentadione were identified as the major oxidation products of curcumin. Anjomshoa *et al.* (2017) evaluated the radical-curcumin reactions towards various reactive oxygen radicals, including $HO^{\bullet}$, $CH_3O^{\bullet}$, $HOO^{\bullet}$, and $O_2^{\bullet-}$ *via* four known mechanisms: SET, RAF, SPLET, and HAT in water and n-octanol solutions in calculating standard Gibbs free energies (DG^0 at 298K) using the BMK/6-311+G(d,p) level of theory (Anjomshoa et al., 2017). The results showed that the HAT mechanism was always more dominant than RAF, SPLET, and SET. And the radical additions toward the double bonds C1=C2 and C6=C7 are more favourable than the ones at C3=C4 (Figure 1). However, these computational works were limited only to the thermodynamics aspect and did not investigate the kinetics of reactions.

The reaction kinetics of curcumins with the ROS were only investigated by the work of Galano *et al.* (2009) (Galano et al., 2009). Indeed, the influence of tautomerism and acid-base equilibrium on the thermodynamics and kinetics of radical scavenging reactions of curcumin (*i.e.*, 1,7-bis(4-hydroxy-3-methoxyphenyl)-1,6-heptadiene-3,5-dione) toward methoxy radical ($CH_3O^{\bullet}$) in water and benzene solvents at the at B3LYP/6-311+G(d,p) level of theory combined with the IEF-PCM solvent model (Galano et al.,

2009). As a result, curcumin exists almost exclusively in its enol form in benzene solution and 99.5 % enol - 0.5 % keto in water solution. In terms of reaction kinetics, the reaction of curcumin with $CH_3O^{\bullet}$, and likely with other alkoxyl radicals, is governed by the HAT mechanism, which agrees with the experimental observation of Barclay *et al.*(Barclay et al., 2000). The overall rate constants for the curcumin + $CH_3O^{\bullet}$ reaction are proposed to be 1.16×10^{10} and 5.52×10^{9} L mol^{-1} s^{-1} in benzene and water solutions, respectively. In water, the hydrogen atom transfer (HAT) mechanism was reported to be more predominant than the radical addition one (RAF).

Although the antioxidant properties of curcumin and its derivatives have been mainly investigated by using various computational approaches based on Density functional theory (DFT), a systematical study is still needed to explore from the electronic structures to the intrinsic parameters and thermodynamics and kinetics of reaction towards reactive free radicals, especially the hydroperoxyl $HOO^{\bullet}$ radical, which is the standard reactive oxygen species (ROS).

Thus, this work aims to systematically evaluate the free radical scavenging activities of curcumin toward the HOO radical in various solvents with different polarities (*i.e.*, water and pentyl ethanoate - PEA). Geometrical and electronic structures of keto-enol and diketone forms of curcumin were first investigated. Different intrinsic parameters, including bond dissociation enthalpies (BDE), ionization potential (IP), and proton affinities (PA), were then calculated to rapidly screen the antioxidant properties. The influence of the acid-base equilibrium and the tautomerism on the reaction rates of curcumin towards HOO radicals was finally investigated in both solutions studied. The overall rate constants of curcumin-HOO radicals were also proposed, considering both influences.

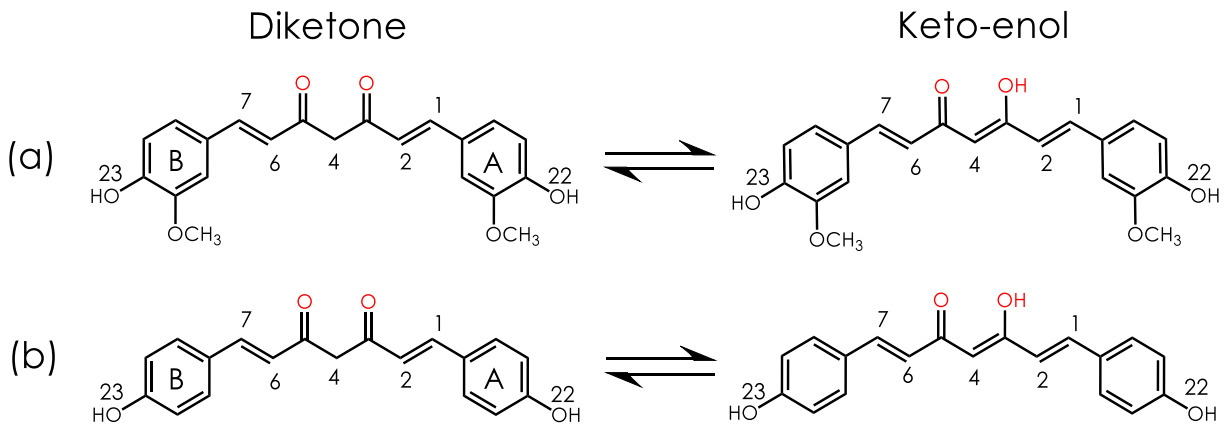

Figure 1. Diketone and keto-enol tautomer structure of (a) Cur-I and (b) Cur-III.

2. Computational details

Gaussian 16 Revision C.01 package (Frisch et al., 2016) was used for all calculations in the framework of Density functional theory (DFT). The geometrical and electronic structures, thermodynamics, and kinetics of the neutral and ionic species were investigated using the M06-2X functional (Zhao and Truhlar, 2008) combined with the 6-31+G(d,p) basis set (Feller, 1996; Pritchard et al., 2019; Schuchardt et al., 2007). The accuracy of the obtained energies was improved with the highest Pople basis set 6-311++G(3df,3pd). These computational approaches have been successfully applied to different molecular systems in recent studies (Dao et al., 2023; K. Al Rawas et al., 2023; Ngo et al., 2023). A scaling factor of 0.952 was applied for the vibrational frequency calculations(Alecu et al., 2010). The influence of the solvents, including water (ε=78.3553) and pentyl pentanoate (PEA, ε=4.7297), was mimicked by employing the solvation model based on the quantum mechanical charge density of a solute molecule interacting with a continuum description of the solvent (SMD) (Marenich et al., 2009). The conformational distribution of the studied compounds was scanned by running the MSTor code (Chen et al., 2023).

The influence of acid-base equilibrium on the HOO radical scavenging activities in the solvents was considered. In the lipid media represented by the PEA solvent, all the studied compounds were assumed to exist in the neutral form. At the same time, in the polar environment (*i.e.*, water), there may be three different deprotonation sites located in the hydroxyl or methylene groups (**Figure 1**). The acid dissociation constants (pKa) were thus computed using semi-empirical models proposed by Rebollar-Zepeda *et al.* for the phenolic derivatives (Rebollar-Zepeda et al., 2011). The antioxidant mechanism and kinetics of the neutral and three anionic forms were then predicted via three standard processes, including hydrogen transfer (HT), radical adduct formation (RAF), and single electron transfer (SET). The pre-reactive complexes scheme proposed by Singleton and Cvetanovic (Singleton and Cvetanovic, 1976) was used for the kinetic calculations of HT and RAF reactions. Details of calculation procedures can be found elsewhere (Dao et al., 2023; K. Al Rawas et al., 2023; Ngo et al., 2023). Intrinsic reaction coordinate (IRC) calculations using the Hessian-based predictor-corrector (HPC) integrator (Dykstra, 2005; Hratchian and Schlegel, 2005, 2004) were performed to confirm whether the imaginary frequency corresponds to the appropriate motion along the reaction coordinates. The Gaussian Post Processor (GPOP) program (Miyoshi, 2022) was used to compute the rate constants of all the reactions. The Gibbs free energy of activation of the SET reaction was computed based on Marcus's theory(Marcus, 1957a, 1957b, 1956). The apparent diffusion-corrected rate constant in the solvents was calculated using Collin-Kimball theory (Collins and Kimball, 1949) and the steady-state Smoluchowski rate constant(Smoluchowski, 1918).

Finally, the overall rate constants ($k_{overall}$) were calculated as the sum of the rate constant for HT (k_{HT}), RAF (k_{RAF}), and SET (k_{SET}) reaction in considering the molar fractions of each acid-base form and the ones of each tautomerism form *via* following reactions (eq. 1):

$$k_{overall} = F_{diketon} \times \sum_i f_i \times k_{tot}^i + F_{keto\text{-}enol} \times \sum_i f_i \times k_{tot}^i \text{ ; (eq. 1)}$$

where *i* denotes the neutral, monoanionic, dianionic, and trianionic forms of curcumin I and III. k_{tot} is the total rate constants of three studied mechanisms (*i.e.*, HT, RAF, and SET), $k_{tot} = k_{HT} + k_{RAF} + k_{SET}$. $F_{diketon}$ and $F_{keto\text{-}enol}$ are the molar fractions of the diketone and keto-enol forms of curcumin.

3. Results and Discussion

3.1. Structure and electronic properties

Figure 2 demonstrates the optimized geometry and electronic structure of the most stable diketone and keto-enol tautomers of Cur-I and Cur-III in water; the ones in PEA are shown in **Figure S1** (**ESI** file).

Regarding the geometrical structures, the diketone tautomer has a V-shape structure with the methylene group (-CH_2-) as the center, while the keto-enol one represents a quasi-planar form favoring strong delocalization of electron densities. The Cur-I and Cur-III have two phenolic –OH groups, which may play roles as hydrogen donating sites. Moreover, the methylene group of the diketone tautomer may also be radical attacking sites *via* the HT process. The diketone form possesses two double bonds, while the keto-enols have three double bonds, which are the reactive sites for RAF reactions. Regarding the frontier orbitals distribution, it is expected that the HOMO and LUMO will mainly locate at C=C bonds and phenyl rings, which may be potential for the RAF reaction. For the ESP map, the most negative atomic zones of the diketone tautomer are found at the C=O group and the phenyl rings. Meanwhile, the most negative regions in keto-enol tautomer spread throughout the whole molecule chain. Conversely, the most positive atomic zones mainly focus on the phenolic -OH and -OCH_3 functional groups.

3.2.Intrinsic thermochemical parameters

Table 1 presents some intrinsic thermochemical properties, including bond dissociation enthalpies (BDE), proton affinity (PA), and ionization potential (IP) of the diketone and keto-enol tautomers of Cur-I and Cur-III in the gas phase and PEA solvent.

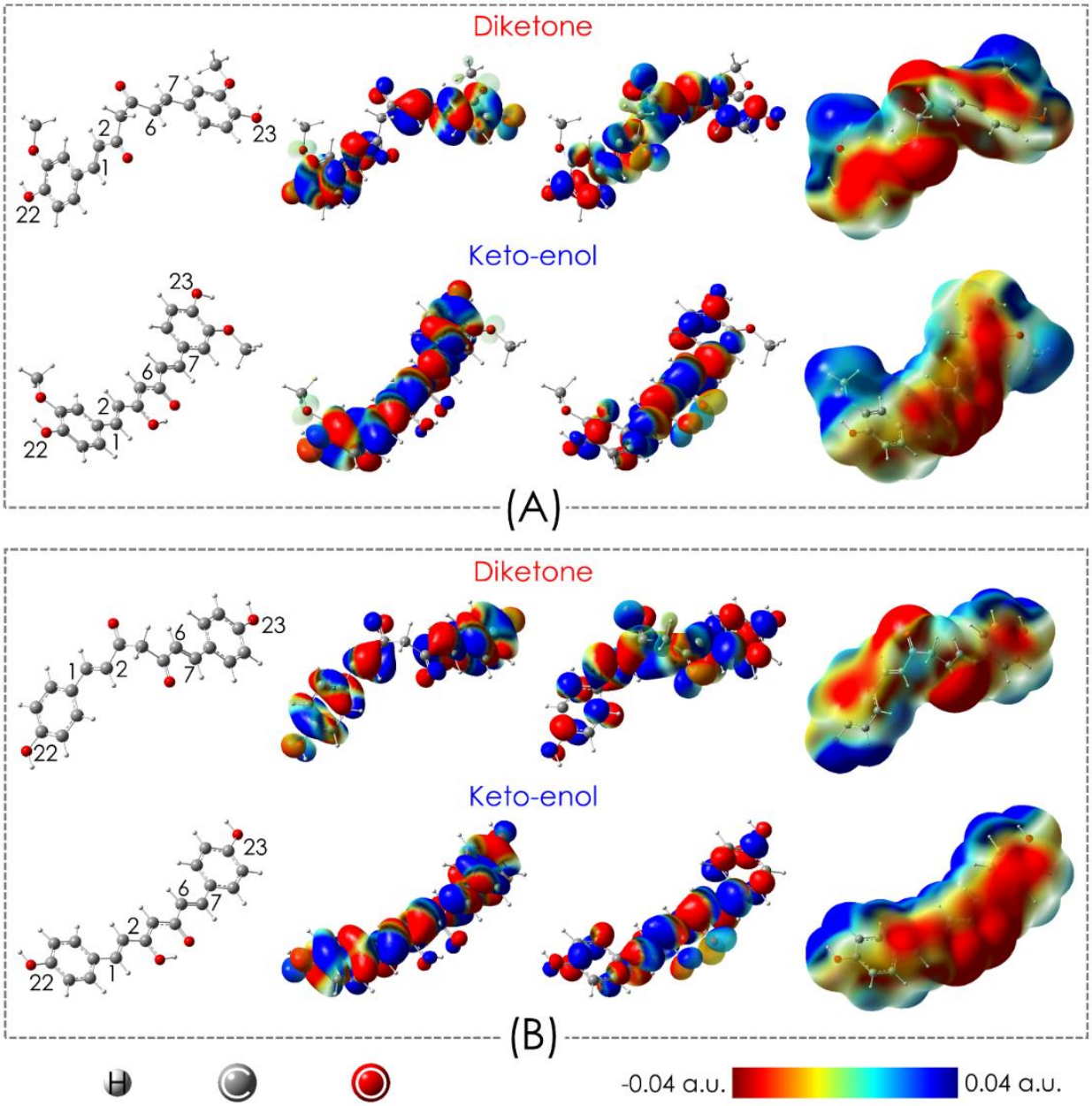

Figure 2. Optimized geometries, HOMOs, LUMOs and ESP maps of diketone and keto-enol tautomers of Cur-I (A) and Cur-III (B) in water.

All the studied compounds favourably dissociate, forming anionic forms and donating protons in water. The values of PA are remarkably lower than the ones of BDE and IP. For example, regarding the Cur-I compounds, the lowest PA values of the diketone in water are 124.1, 128.0, and 129.5 kJ mol^{-1} obtained at the C4H, O22H, and O23H positions, respectively. Meanwhile, the lowest BDE values of this compound are 354.8, 357.3, and 389.3 kJ mol^{-1} at the O22H, O23H, and C4H, respectively. Similarly, the lowest PAs of the keto-enol in water are found at the phenolic hydroxyl groups, *i.e.*, 131.4 (O23H), 132.2 (O22H), and

135.2 kJ mol^{-1} (O20H), while its lowest BDE values are much higher, *i.e.*, 351.3 (O23H), 351.5 (O22H) and 364.5 kJ mol^{-1} (O20H). Their IP values are broadly higher than the PA and the BDE (*i.e.,* 527.4 and 518.5 kJ mol^{-1} for the diketone and the keto-enol, respectively). Thus, the diketone and keto-enol of Cur-I may easily donate protons *via* three steps characterized by different acid dissociation constants (pKa values), as presented in the next section. Similar observations are also recognized for the Cur-III in both the tautomer forms. The antioxidant properties of the studied compounds in water depend on the activities of their anionic forms. The lowest PA values compared with the BDEs and IPs suggest that proton transfer and electron transfer in a sequential or coupled manner may be dominant processes. This observation is like the one in the lipid media.

Table 1: The BDE, PA, and IP of the diketone and keto-enol tautomers of Cur-I and Cur-III (Unit in kJ mol^{-1}).

Position	Curcumin I						Curcumin III					
	Diketone			Keto-enol			Diketone			Keto-enol		
	BDE	PA	IP	BDE	PA	IP	BDE	PA	IP	BDE	PA	IP
WATER												
-			**527.4**			**518.5**			**543.6**			**528.9**
O22H	357.3	128.0		351.5	**131.4**		**374.9**	129.1		**368.3**	133.0	
O23H	**354.8**	129.5		**351.3**	132.2		**374.9**	129.1		371.8	**132.6**	
O20H	-	-		464.5	135.2		-	-		463.0	137.1	
C1H	-	292.6		-	-		-	307.0		-	-	
C2H	-	234.5		-	-		-	223.7		-	-	
C4H	389.3	**124.1**		464.9	293.1		388.5	**124.4**		495.5	293.6	
C6H	-	212.6		-	-		-	223.7		-	-	
C7H	-	302.2		-	-		-	307.2		-	-	
C24H	421.1	-		421.4	-		-	-		-	-	
C25H	419.0	-		421.0	-		-	-		-	-	
PEA												
-			**536.6**			**550.8**			**579.8**			**560.4**
O22H	356.1	250.7		352.3	**250.3**		**365.7**	**239.9**		362.6	240.4	
O23H	**353.5**	251.9		**351.7**	252.9		**365.7**	**239.9**		**360.0**	**239.7**	
O20H	-	-		463.3	283.4		-	-		462.2	283.1	
C1H	-	411.4		-	-		-	420.3		-	-	
C2H	-	367.4		-	-		-	366.7		-	-	
C4H	384.0	**248.1**		490.1	418.3		384.1	247.8		490.0	418.0	
C6H	-	354.2		-	-		-	366.7		-	-	
C7H	-	412.6		-	-		-	420.3		-	-	
C24H	415.6	-		415.7	-		-	-		-	-	
C25H	416.2	-		416.0	-		-	-		-	-	

3.3.Acid-base equilibria

Acid-base equilibria represent a crucial role in the free radical scavenging activities of the potential antioxidant compound. We have computed the acid dissociation constants *via* pKa values of three proton dissociation steps for all the studied curcumins in the aqueous phase (**Table S1, ESI** file). The three most favored deprotonation sites of each studied compound can be seen in **Table S1**. The obtained pKa values

for the three respective dissociation steps of the diketone are 7.1, 8.9, and 9.2 for Cur-I and 7.3, 8.8, and 9.2 for Cur-III. The corresponding values of the keto-enol are 7.9, 8.7, and 9.0 for Cur-I and 7.9, 9.0, and 9.1 for Cur-III. It allows deducing that the neutral and monoanionic consist in the most preponderant forms at the physiological condition (pH being 7.4). However, the dianionic and trianionic forms are also found with the lower molar fraction.

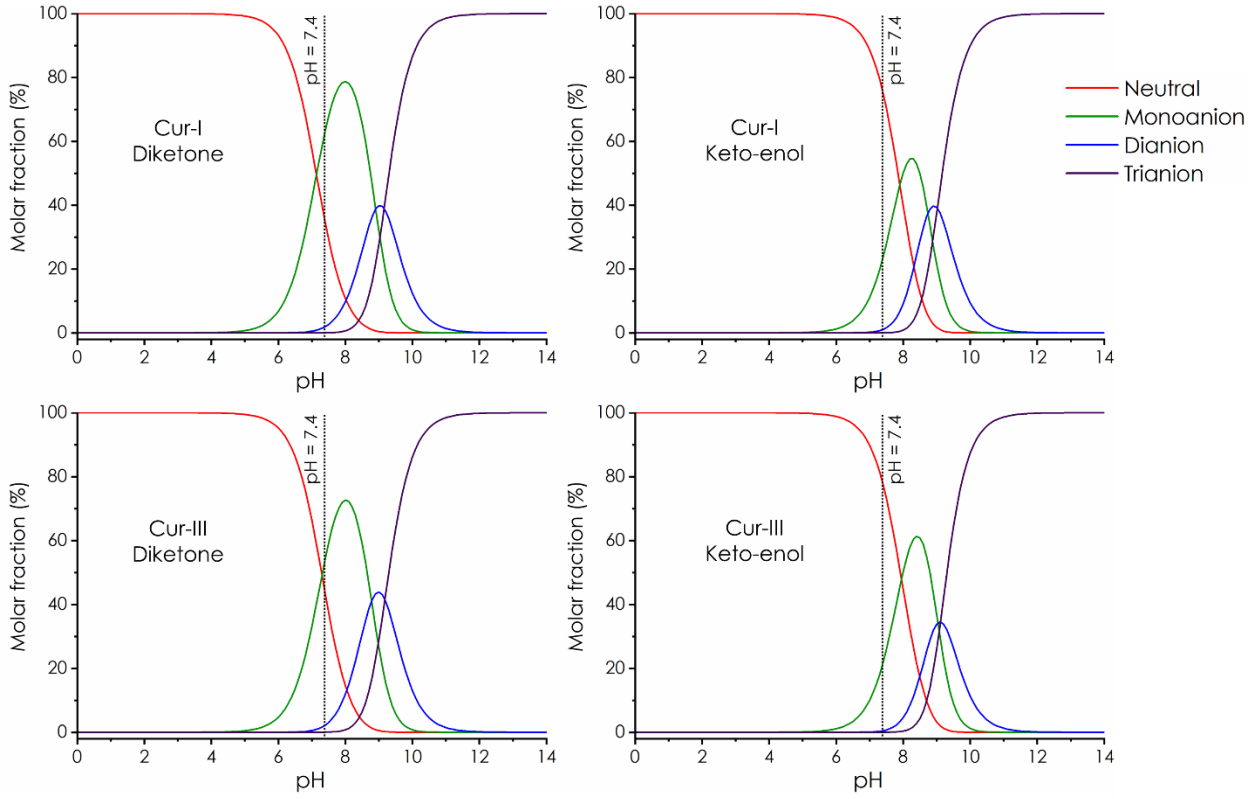

Figure 3: Molar fraction (%) of the neutral and anionic species of Cur-I and Cur-III in the diketone and keto-enol tautomer as a function of pH conditions.

Figure 3 displays the evolution of molar fraction for different existing forms of the studied compounds. It can be observed that at the acidic condition (pH inferior of 7.0), the diketone and keto-enol tautomer of Cur-I and Cur-III are almost available in the neutral and monoanionic forms, while at the basic conditions (pH superior of 7.0) further deprotonations are observed in finding not only the neutral and monoanion but also dianion and trianion. **Table S2** (**ESI** file) resumes the molar fraction of the co-existing forms at the pH=7.4 conditions. At the physiological conditions, the diketone of Cur-I, as an example, exists in the aqueous phase mostly in the monoanion form (63.44%), being much higher than the neutral (34.54%), the dianion (1.99%) and trianion (0.33%). Meanwhile, its keto-enol tautomer is almost present in the neutral form (75.10%) with a smaller portion of monoanion (23.78%), dianion (1.09%) and trianion (0.03%). Similar observations are found for the Cur-III compounds. To have a complete picture of the antioxidant

activity of Cur-I and Cur-II, all the four existing forms of both the tautomers, including neutral, monoanion, dianion, and trianion, will be evaluated in the reaction with the HOO radical in water.

3.4. Free radical scavenging mechanism

a. HOO• free radical scavenging mechanism of Cur-I

Figure 4 displays transition states (TSs) optimized structures of hydrogen abstraction (Abs) reactions at the phenolic –OH groups obtained in water and PEA media and radical addition (Add) ones at different carbon-centers of double bonds in the neutral and monoanionic forms for the diketone of Cur-I. Similar figures for the dianionic and trianionic species are also presented in **Figure S2** (**ESI** file).

For the abstraction reactions, the bond distances (HOO)O···H(HO-) fluctuate around 1.36 – 1.39 Å and 1.31 – 1.32 Å in water and PEA, while the -O···H lengths of the phenolic hydroxyl group are about 1.06 - 1.07 Å and 1.09 – 1.10 Å, respectively, and the O-H-O bond angles are about 160 - 161°. For the addition ones, the interactive lengths C···O(HOO) vary in the range of 1.90 – 2.01 Å in water and about 1.93 – 1.97 Å in PEA solvent.

Figure 5 displays the ZPE-corrected relative enthalpy profile at 0 K (ΔH_{0K}) condition for the hydrogen abstraction (Abs) and radical addition (Add) reactions of the Cur-I compound in water and PEA media.

In water, the monoanion (MoA) of the diketone and the neutral (Neu) form of the keto-enol tautomer are chosen to present as representative cases because of their highest molar fractions (63.44 and 75.10%, **Table S3**). The PESs of the other anionic forms are shown in **Figure S**xx (**ESI** file). It is expected that the H-Abs reaction between the MoA diketone with the radical occurs essentially at the phenolic O22H and O23H groups *via* four steps (*i.e.*, reactant complexes – RC, transition states – TS, product complexes – PC and separated products – RAD) with similar relative enthalpy profiles (ΔH_{0K}). Indeed, the ΔH_{0K} values for the TS are 29.4 and 29.5 kJ mol^{-1} for TS22 and TS23, respectively, while the values of the products (RAD22 and RAD23) are -26.8 and -27.5 kJ mol^{-1}. On the other hand, the radical addition (Add) process takes place in three consecutive steps, including RC, TS, and PC. Five radical Add reactions are observed at the C1, C2, C4, C6, and C7 of the MoA of diketone. The Add reaction of HOO radical at the C4 position represents the most preponderant reaction, with the lowest TS enthalpy value being 18.3 kJ mol^{-1} (TS4) and the most negative value of the product (PC4, -48.2 kJ mol^{-1}). Meanwhile, the Add processes at C1 and C7, near the phenolic rings, occur with the highest TS enthalpies being 44.7 (TS7) and 45.0 (TS1). The Neu keto-enol tautomer displays lower free radical scavenging activities than the MoA diketone with higher enthalpies of TSs and products. For example, the ΔH_{0K} values for the TS22 and TS23 of the H-Abs reaction are equal to 33.0 and 33.6 kJ mol-1, which are all higher than the corresponding values of the MoA diketone, whereas

the ones for RAD22 and RAD23 are of -22.5 and -22.4 kJ mol^{-1}, respectively. Similarly, the most preponderant Add reaction is observed at the C6 position with higher relative enthalpies for TS6 (40.7 kJ mol^{-1}) and PC6 (-40.0 kJ mol^{-1}).

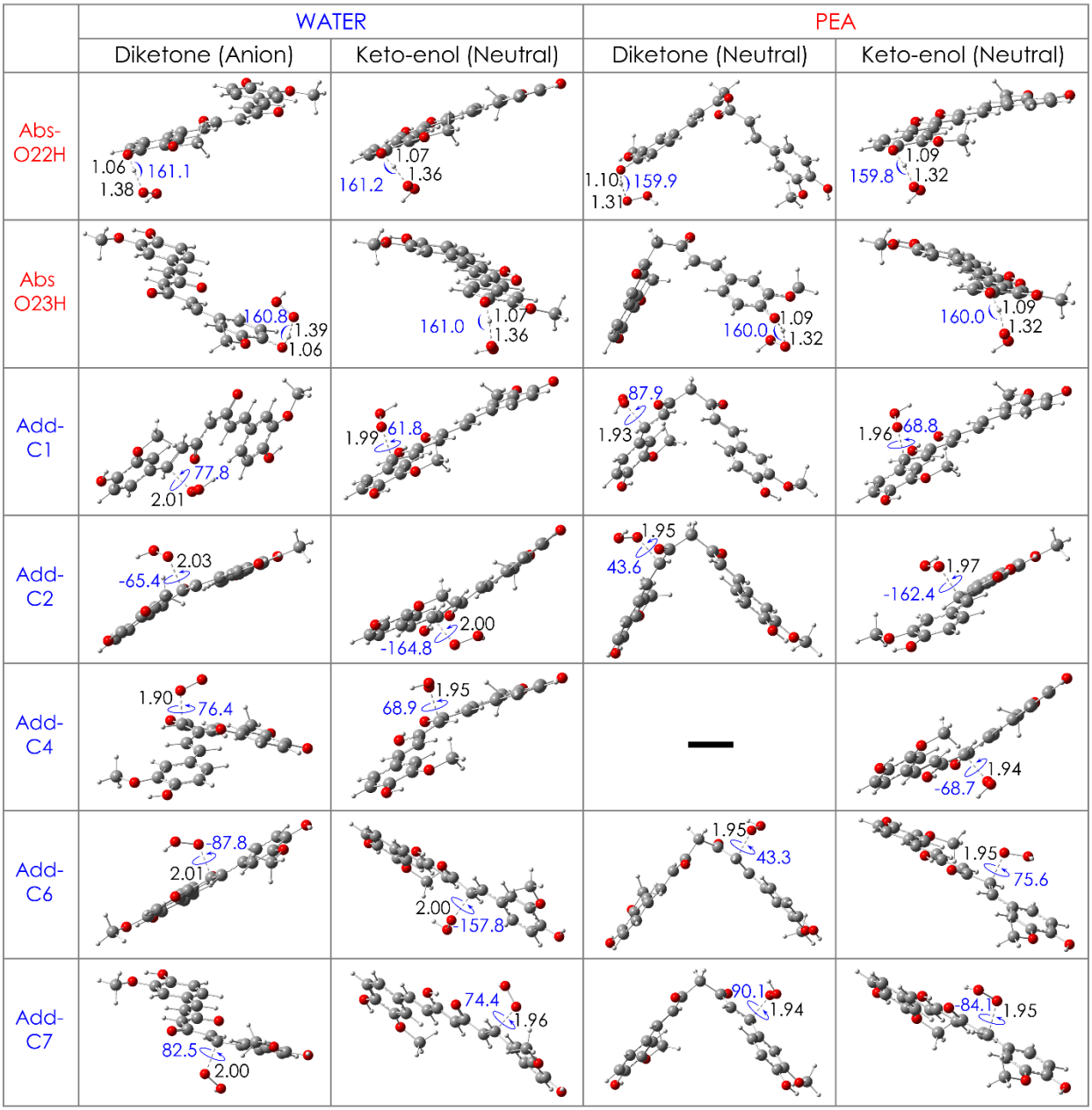

Figure 4: Transition states (TSs) of HT and RAF reactions between the most stable forms of diketone and keto-enol tautomer of Cur-I in water and PEA. The numbers in black are the interactive distance (in Å), and the ones in blue are bond angles and dihedral angles (º) for H-abstraction (Abs) and addition (Add) reactions, respectively.

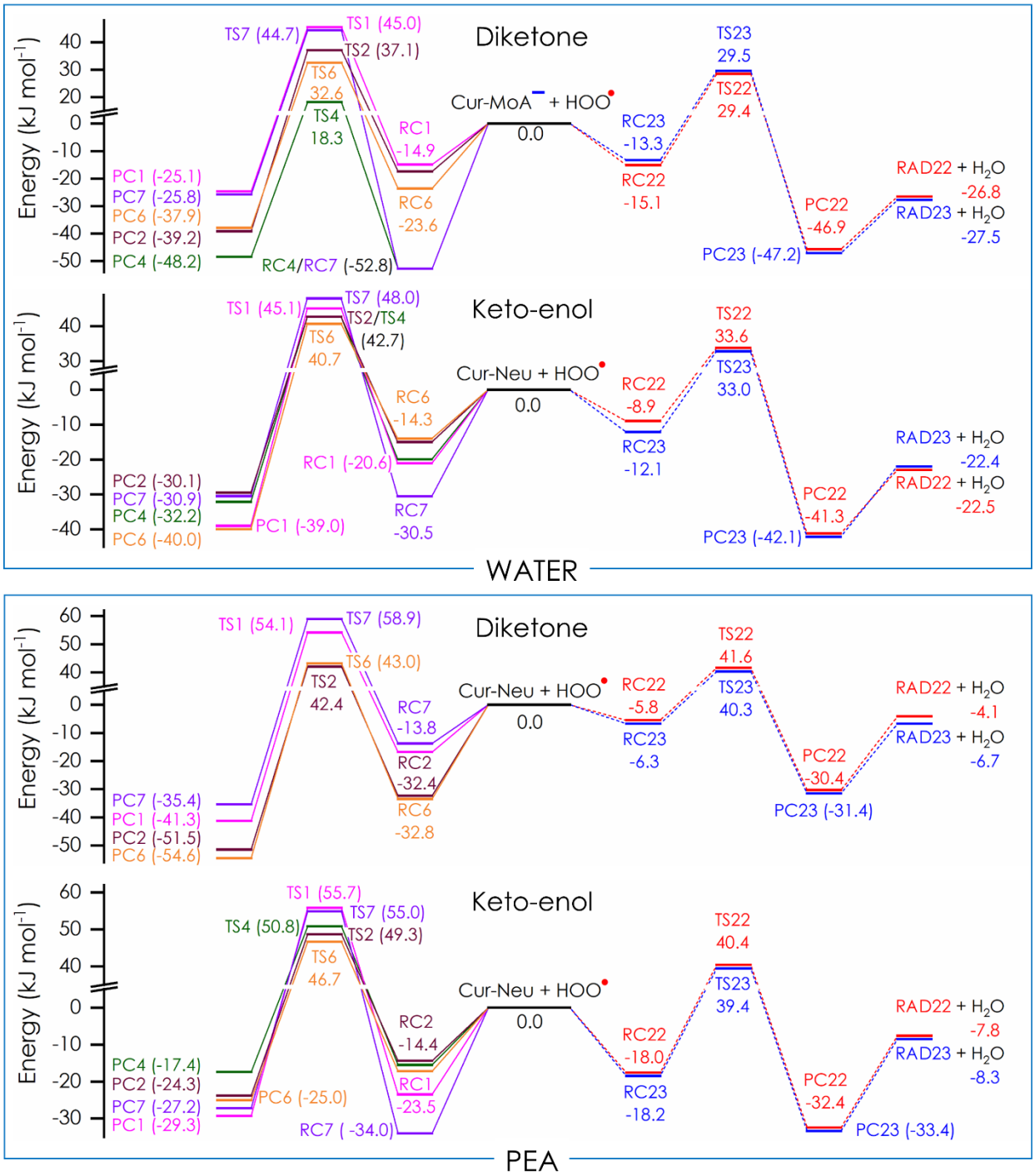

Figure 5: ZPE-corrected relative enthalpy profile at 0 K (ΔH_{0K}) for abstraction (right) and addition (left) reactions initiated by HOO• radical of Cur-I in water and PEA.

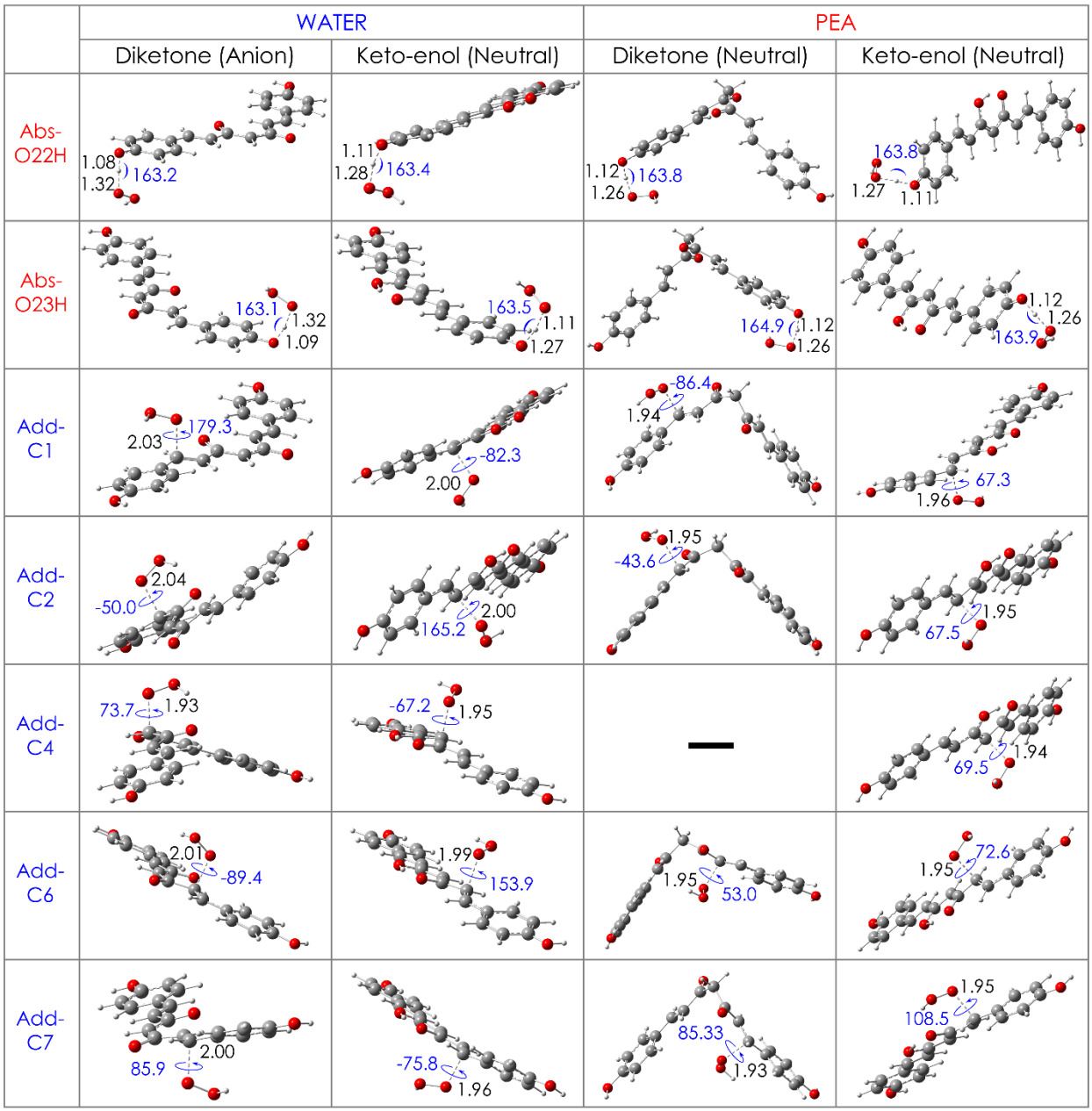

Figure 6: Transition states (TSs) of HT and RAF reactions between the most stable forms of diketone and keto-enol tautomer of Cur-III in water and PEA. The numbers in black are the interactive distance (in Å), and the ones in blue are bond angles and dihedral angles (º) for H-abstraction (Abs) and addition (Add) reactions, respectively.

In PEA solvent (a lipid-like media), both tautomers are present in the neutral form. Their radical scavenging activities are less favourable than the ones in the aqueous phase. For example, the relative enthalpies of TS22 and TS23 for the Abs reactions of the Neu diketone are 41.6 and 40.3 kcal mol^{-1}, respectively, about 10 kcal mol^{-1} higher than the ones in water. Similar values of 41.6 and 40.3 kcal mol^{-1}

are observed for the TS22 and TS23 of the Neu keto-enol. The same trend is also recognized for the Add processes in PEA (**Figure 5**).

b. HOO• free radical scavenging of Cur-III

The optimized structures of TSs for Abs and Add reaction of Cur-III in the diketone and keto-enol forms with HOO radical in water and PEA are presented in **Figure 6**. We only present the TS structures of the MoA for diketone and the Neu for the keto-enol tautomer that occupy the most significant molar fractions in the aqueous phase, *i.e.*, 54.38 % and 77.56 %, respectively. The structures of other anionic forms are displayed in **Figure S**xx (**ESI** file). Conversely, only the Neu form of both the tautomers exists in the PEA solvent.

As can be seen in **Figure 6**, the -O···H bond lengths of the phenolic hydroxyl group vary from about 1.08 to 1.11 Å for the Abs reactions at O22H and O23H positions in water, whereas the ones in PEA are about 1.11 to 1.12 Å. The (HOO)O···H(HO-) distances are from 1.27 to 1.32 Å for the Abs reactions in water and from 1.26 to 1.27 Å in PEA. The O-H-O bond angles vary from 163 to 165° in both media. Regarding the Add processes, the C···O(HOO) interactive distances are from 1.93 to 2.04 Å in water and from 1.93 to 1.96 Å in PEA.

The ZPE-corrected relative enthalpy profiles at 0 K condition for the reactions of Cur-III and HOO radicals in water and PEA are shown in **Figure 7**. Like the Cur-I, the Abs reactions of the Neu keto-enol in water have higher relative enthalpy values (ΔH_{0K}, 48.7, and 50.2 kJ mol^{-1} for TS22 and TS23, respectively) than the ones of the MoA diketone tautomer (43.0 and 43.3 kJ mol^{-1}). In addition, the lowest relative enthalpy of TS for the Add reaction of the Neu keto-enol (41.8 kJ mol^{-1} for TS6) is also higher than that of the MoA diketone (15.9 kJ mol^{-1} for TS4). In PEA, TSs of Abs reaction for the Neu diketone conversely have higher relative enthalpies (46.4 and 45.5 kJ mol^{-1} for TS22 and TS23, respectively) than the ones for the Neu keto-enol (43.7 and 44.7 kJ mol^{-1}). Conversely, the Add reaction for the Neu diketone has a lower ΔH_{0K} value of TS than the Neu keto-enol. The lowest ΔH_{0K} value of the Neu diketone is found with the reaction at C6 (TS6, 38.2 kJ mol^{-1}), which is lower than the one of the Neu keto-enol (TS6, 47.4 kJ mol^{-1}).

Thus, regarding the thermodynamic aspect, the observations are similar for the Cur-I and Cur-III. In water, the comparison of the relative enthalpy profiles of diketone and keto-enol is not evident because of the different molar fractions of the neutral and anionic species of each tautomer. In PEA, the Neu diketone has higher relative enthalpies of the Abs TS but lower relative enthalpies of the Add TS than the Neu keto-enol. In the next section, the kinetic aspect will be considered to provide more evidence of the influence of tautomerism on the radical scavenging activities of Cur-I and Cur-III.

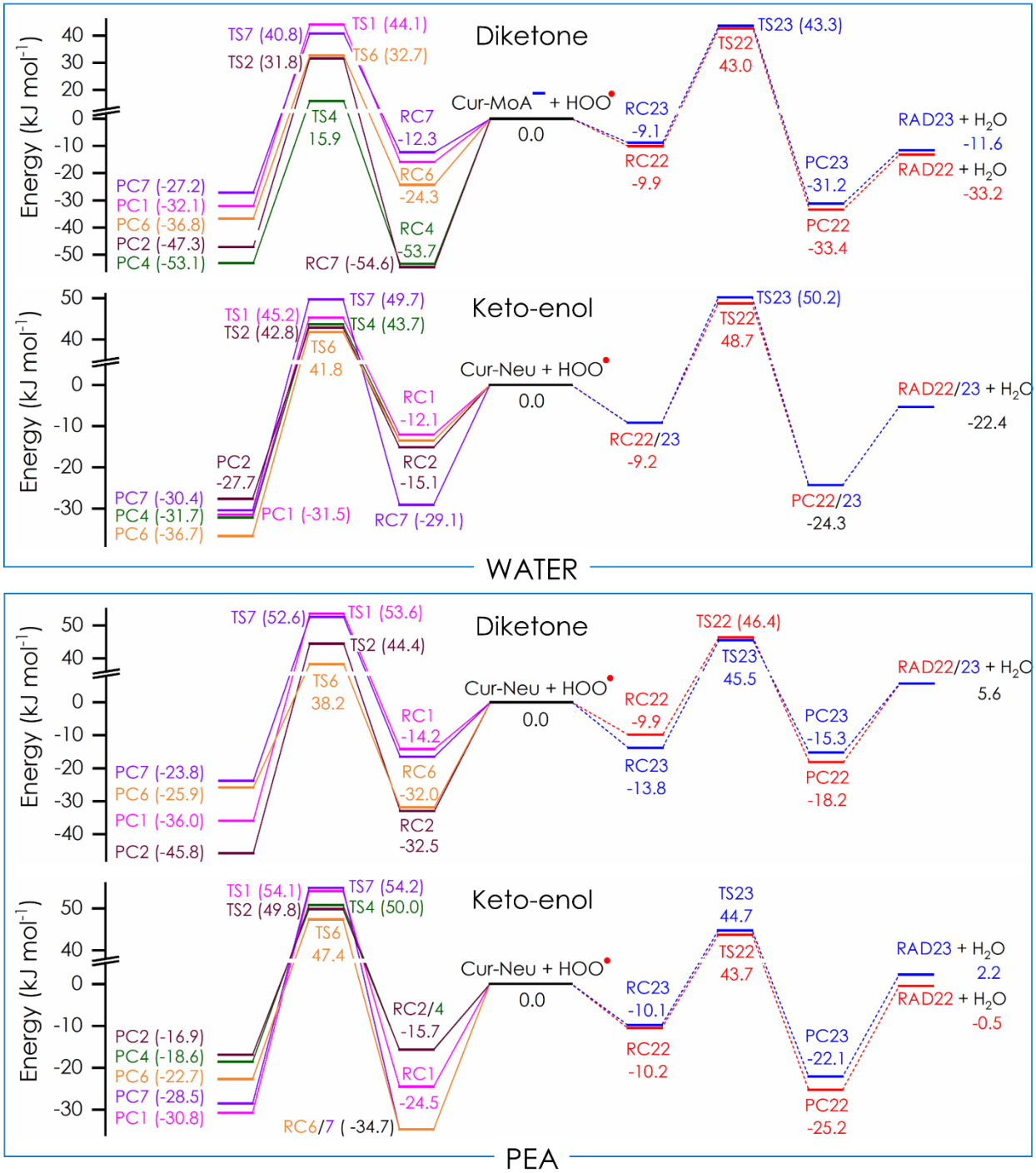

Figure 7: ZPE-corrected relative enthalpy profile at 0 K (ΔH_{0K}) for abstraction (right) and addition (left) reactions initiated by HOO• radical of Cur-III in water and PEA.

3.5. Kinetics of reactions

Kinetics of reactions between the neutral and anionic forms of the diketone and keto-enol compounds have been computed to get a more reliable prediction of free radical scavenging activities. For that purposes, Gibbs free energy of activation ($\Delta G^{\ddagger}$, kJ mol^{-1}) and reaction ($\Delta_r G^0$, kJ mol^{-1}), thermal rate constant (k_T, M^{-1} s^{-1}), diffusion rate constant (k_D, M^{-1} s^{-1}), apparent rate constant (k_{app}, M^{-1} s^{-1}) were calculated for the diketone and keto-enol of Cur-I (**Tables 2** and **3**) and the ones of Cur-III (**Tables 4** and **5**). The apparent rate constants were then corrected by the molar fraction of Cur-I and Cur-III (k_{app}^{Mf}, M^{-1} s^{-1}), respectively.

Table 2 resumes all kinetics parameters of the reaction between the diketone of Cur-I with HOO radical in PEA and water. In water, the neutral and monoanion forms essentially react with the HOO radical *via* FHT at the O22H and O23H positions and RAF reactions at the C4 atom. In contrast, the favourable mechanisms for the dianion and trianion consist of the SET process. The FHT reactions at O22H and O23H occur with the corrected apparent rate constants (k_{app}^{Mf}) being 1.45×10^3, 2.63×10^3 M^{-1}s^{-1} and 2.31×10^4, 3.80×10^3 M^{-1} s^{-1} for the neutral and monoanion forms. In contrast, the rate constant value of the RAF at the C4 position of monoanion is equal to 1.44×10^3 M^{-1} s^{-1}. These mechanisms become negligible for the dianion and trianion foms, of which the SET process plays a crucial role, with the rate constants being 1.60×10^8 and 2.65×10^6 M^{-1} s^{-1}, respectively.

The similar observations can be recognized for the keto-enol tautomer of Cur-I in both water and PEA solvents (**Table 3**). In water, the hydrogen abstraction consists in the most predominant process for the neutral and monoanionic forms (*i.e.*, 3.01×10^3/3.86×10^3 M^{-1}s^{-1} and 3.72×10^3/4.90×10^3 M^{-1}s^{-1}, respectively for the O22H/O23H abstraction reactions). At the same time, the single electron transfer is the most dominant reaction for dianionic and trianionic forms (*i.e.*, 9.10×10^7 and 2.22×10^6 M^{-1}s^{-1}, respectively). Furthermore, it is noteworthy that the rate constants of the studied reactions of the keto-enol tautomers are all higher than the ones of the diketone compound.

Table 2: The Gibbs free energy of activation ($\Delta G^{\ddagger}$, kJ mol^{-1}) and reaction ($\Delta_r G^0$, kJ mol^{-1}), thermal rate constant (k_T, M^{-1} s^{-1}), diffusion rate constant (k_D, M^{-1} s^{-1}), apparent rate constant (k_{app}, M^{-1} s^{-1}), apparent rate constant corrected by the molar fraction of Cur-I (k_{app}^{Mf}, M^{-1} s^{-1}), and branching ratio (Γ, %) of the reactions between the HOO$^{\bullet}$ radical and the diketone tautomer of Cur-I in water and PEA.

Form	Position	$\Delta G^{\ddagger}$	$\Delta_r G^0$	k_T	k_D	k_{app}	k_{app}^{Mf}	Γ
WATER								
				Abstraction reaction				
	O22H	-18.2	80.3	4.20×10^{3}	2.39×10^{9}	4.20×10^{3}	1.45×10^{3}	0.00
	O23H	-18.9	80.3	7.61×10^{3}	2.58×10^{9}	7.61×10^{3}	2.63×10^{3}	0.00
				Addition reaction				
Neutral	C1	24.4	95.3	5.75×10^{-3}	1.95×10^{9}	5.75×10^{-3}	1.99×10^{-3}	0.00
(f_i = 34.54 %)	C2	15.2	86.6	1.42×10^{-1}	1.98×10^{9}	1.42×10^{-1}	4.91×10^{-2}	0.00
	C6	11.5	84.5	3.03×10^{-1}	1.99×10^{9}	3.03×10^{-1}	1.14×10^{-1}	0.00
	C7	27.2	96.9	2.94×10^{-3}	1.96×10^{9}	2.94×10^{-3}	1.02×10^{-3}	0.00
				Single electron transfer reaction				
		128.8	147.9	1.86×10^{-12}	8.50×10^{9}	1.86×10^{-12}	6.42×10^{-13}	0.00
				Abstraction reaction				
	O22H	-24.1	76.1	3.64×10^{4}	2.40×10^{9}	3.64×10^{4}	2.31×10^{4}	0.00
	O23H	-27.7	77.6	5.99×10^{3}	2.40×10^{9}	5.99×10^{3}	3.80×10^{3}	0.00
				Addition reaction				
	C1	22.7	92.8	1.34×10^{-2}	2.00×10^{9}	1.34×10^{-2}	8.53×10^{-3}	0.00
MonoAnion	C2	11.2	86.0	1.85×10^{-1}	2.02×10^{9}	1.85×10^{-1}	1.17×10^{-1}	0.00
(f_i = 63.44 %)	C4	4.2	62.1	2.28×10^{3}	1.89×10^{9}	2.28×10^{3}	1.44×10^{3}	0.00
	C6	14.6	81.0	1.37×10^{0}	2.02×10^{9}	$1.3.7 \times 10^{0}$	8.68×10^{-1}	0.00
	C7	23.9	91.9	1.94×10^{-2}	1.99×10^{9}	1.94×10^{-2}	1.23×10^{-2}	0.00
				Single electron transfer reaction				
		62.8	62.8	1.52×10^{3}	8.56×10^{9}	1.52×10^{3}	9.62×10^{2}	0.00
				Abstraction reaction				
	O23H	-29.4	75.9	1.89×10^{4}	2.43×10^{9}	1.89×10^{4}	3.76×10^{2}	0.00
				Addition reaction				
	C1	32.1	83.7	4.74×10^{-1}	2.03×10^{9}	4.74×10^{-1}	9.41×10^{-3}	0.00
DiAnion	C2	5.3	61.0	3.27×10^{3}	2.23×10^{9}	3.27×10^{3}	6.50×10^{1}	0.00
(f_i = 1.99 %)	C4	-9.8	59.1	7.25×10^{3}	1.96×10^{9}	7.25×10^{3}	1.44×10^{2}	0.00
	C6	11.4	80.6	1.66×10^{0}	2.04×10^{9}	1.66×10^{0}	3.31×10^{-2}	0.00
	C7	21.0	87.8	1.00×10^{-1}	2.01×10^{9}	1.00×10^{-1}	1.99×10^{-3}	0.00
				Single electron transfer reaction				
		5.0	17.0	1.57×10^{11}	8.47×10^{9}	8.03×10^{9}	1.60×10^{8}	98.35
				Addition reaction				
	C1	22.0	81.1	1.34×10^{0}	2.03×10^{9}	1.34×10^{0}	4.68×10^{-4}	0.00
	C2	-17.6	51.6	1.45×10^{5}	2.35×10^{9}	1.45×10^{5}	5.05×10^{1}	0.00
TriAnion (f_i =	C4	2.7	55.0	3.95×10^{4}	1.90×10^{9}	3.95×10^{4}	1.38×10^{1}	0.00
0.03 %)	C6	5.8	57.8	1.28×10^{4}	2.24×10^{9}	1.28×10^{4}	4.45×10^{0}	0.00
	C7	18.1	82.6	7.13×10^{-1}	2.03×10^{9}	7.13×10^{-1}	2.49×10^{-4}	0.00
				Single electron transfer reaction				
		-2.7	19.1	6.88×10^{10}	8.52×10^{9}	7.58×10^{9}	2.65×10^{6}	1.63
Total							1.62×10^{8}	100.00
PENTYL ETHANOATE								
				Abstraction reaction				
	O22H	-6.73	86.81	1.50×10^{1}	2.65×10^{9}	1.50×10^{1}	1.50×10^{1}	27.95
	O23H	-10.89	84.40	3.85×10^{1}	2.65×10^{9}	3.85×10^{1}	3.85×10^{1}	71.87
Neutral				Addition reaction				
(f_i = 100.00 %)	C1	18.53	98.53	7.28×10^{-4}	2.16×10^{9}	7.28×10^{-4}	7.28×10^{-4}	0.00
	C2	7.63	86.8	6.98×10^{-2}	2.18×10^{9}	6.98×10^{-2}	6.98×10^{-2}	0.13
	C6	22.01	95.57	2.44×10^{-2}	2.29×10^{9}	2.44×10^{-2}	2.44×10^{-2}	0.05
	C7	27.47	99.26	5.26×10^{-4}	2.17×10^{9}	5.26×10^{-4}	5.26×10^{-4}	0.00
Total							5.36×10^{1}	100.00

Table 3: The Gibbs free energy of activation ($\Delta G^{\ddagger}$, kJ mol^{-1}) and reaction ($\Delta_r G^0$, kJ mol^{-1}), thermal rate constant (k_T, M^{-1} s^{-1}), diffusion rate constant (k_D, M^{-1} s^{-1}), apparent rate constant (k_{app}, M^{-1} s^{-1}), apparent rate constant corrected by the molar fraction of Cur-I (k_{app}^{Mf}, M^{-1} s^{-1}), and branching ratio (Γ, %) of the reactions between the HOO$^{\bullet}$ radical and the keto-enol tautomer of Cur-I in water and PEA.

Form	Position	$\Delta G^{\ddagger}$	$\Delta_r G^0$	k_T	k_D	k_{app}	k_{app}^{Mf}	Γ
WATER								
				Abstraction reaction				
	O22H	-25.5	80.1	4.01×10^{3}	2.42×10^{9}	4.01×10^{3}	3.01×10^{3}	0.00
	O23H	-23.0	78.8	5.14×10^{3}	2.42×10^{9}	5.14×10^{3}	3.86×10^{3}	0.00
				Addition reaction				
Neutral	C1	8.9	88.6	7.83×10^{-2}	2.00×10^{9}	7.83×10^{-2}	5.88×10^{-2}	0.00
(f_i = 75.10 %)	C2	16.5	90.3	3.66×10^{-2}	2.01×10^{9}	3.66×10^{-2}	2.52×10^{-2}	0.00
	C4	11.9	89.0	5.12×10^{-2}	1.97×10^{9}	5.12×10^{-2}	3.85×10^{-2}	0.00
	C6	9.2	86.0	1.89×10^{-1}	2.01×10^{9}	1.89×10^{-1}	1.42×10^{-1}	0.00
	C7	17.2	91.9	2.16×10^{-2}	1.97×10^{9}	2.16×10^{-2}	1.62×10^{-2}	0.00
				Single electron transfer reaction				
		142.6	174.3	4.46×10^{-17}	8.45×10^{9}	4.46×10^{-17}	3.44×10^{-17}	0.00
				Abstraction reaction				
	O22H	-29.5	74.4	1.57×10^{4}	2.42×10^{9}	1.57×10^{4}	3.72×10^{3}	0.00
	O23H	-29.7	72.8	2.06×10^{4}	2.42×10^{9}	2.06×10^{4}	4.90×10^{3}	0.01
				Addition reaction				
MonoAnion	C1	21.5	88.4	7.85×10^{-2}	2.01×10^{9}	7.85×10^{-2}	1.87×10^{-2}	0.00
(f_i = 23.78 %)	C2	4.1	78.3	3.85×10^{0}	2.03×10^{9}	3.85×10^{0}	9.14×10^{-1}	0.00
	C4	-4.2	66.9	3.17×10^{2}	1.92×10^{9}	3.17×10^{2}	7.54×10^{1}	0.00
	C6	-2.6	79.0	3.23×10^{0}	2.04×10^{9}	3.23×10^{0}	7.68×10^{-1}	0.00
	C7	8.8	88.7	7.03×10^{-2}	2.08×10^{9}	7.03×10^{-2}	1.67×10^{-2}	0.00
				Single electron transfer reaction				
		66.7	66.7	2.91×10^{2}	8.48×10^{9}	2.91×10^{2}	6.91×10^{1}	0.00
				Abstraction reaction				
	O23H	11.8	75.5	1.78×10^{4}	2.39×10^{9}	1.78×10^{4}	1.95×10^{2}	0.00
				Addition reaction				
	C1	20.4	86.9	1.48×10^{-1}	2.03×10^{9}	1.48×10^{-1}	1.62×10^{-3}	0.00
DiAnion	C2	-8.1	55.6	4.95×10^{4}	2.25×10^{9}	4.95×10^{4}	5.42×10^{2}	0.00
(f_i = 1.09 %)	C4	-12.0	62.8	1.67×10^{3}	1.90×10^{9}	1.67×10^{3}	1.83×10^{1}	0.00
	C6	7.0	78.8	3.18×10^{0}	2.00×10^{9}	3.18×10^{0}	3.48×10^{-2}	0.00
	C7	14.8	88.3	8.30×10^{-2}	1.98×10^{9}	8.30×10^{-2}	9.08×10^{-4}	0.00
				Single electron transfer reaction				
		3.2	16.0	2.35×10^{11}	8.62×10^{9}	8.31×10^{9}	9.10×10^{7}	97.60
				Addition reaction				
	C1	20.4	87.2	1.23×10^{-1}	2.05×10^{9}	1.23×10^{-1}	3.24×10^{-5}	0.00
	C2	-7.4	55.0	6.75×10^{4}	2.26×10^{9}	6.75×10^{4}	1.77×10^{1}	0.00
TriAnion	C4	2.7	61.9	2.41×10^{3}	1.89×10^{9}	2.41×10^{3}	6.32×10^{-1}	0.00
(f_i = 0.03 %)	C6	-1.3	54.0	5.87×10^{4}	2.24×10^{9}	5.87×10^{4}	1.54×10^{1}	0.00
	C7	21.4	85.3	2.51×10^{-1}	2.01×10^{9}	2.51×10^{-1}	6.59×10^{-5}	0.00
				Single electron transfer reaction				
		0.4	13.9	5.57×10^{11}	8.58×10^{9}	8.45×10^{9}	2.22×10^{6}	2.38
Total							9.32×10^{7}	100.00
PENTYL ETHANOATE								
				Abstraction reaction				
	O22H	-6.32	89.55	1.91×10^{1}	2.63×10^{9}	1.91×10^{1}	1.91×10^{1}	47.54
	O23H	-6.30	88.88	2.11×10^{1}	2.66×10^{9}	2.11×10^{1}	2.11×10^{1}	52.45
				Addition reaction				
Neutral	C1	18.31	102.37	2.95×10^{-4}	2.17×10^{9}	2.95×10^{-4}	2.95×10^{-4}	0.00
(f_i = 100.00 %)	C2	28.01	98.46	1.33×10^{-3}	2.18×10^{9}	1.33×10^{-3}	1.33×10^{-3}	0.00
	C4	33.44	98.48	1.19×10^{-3}	2.14×10^{9}	1.19×10^{-3}	1.19×10^{-3}	0.00
	C6	20.40	96.43	2.88×10^{-3}	2.16×10^{9}	2.88×10^{-3}	2.88×10^{-3}	0.00
	C7	27.10	107.52	4.20×10^{-5}	2.16×10^{9}	4.20×10^{-5}	4.20×10^{-5}	0.00
Total							4.02×10^{1}	100.00

Table 4: The Gibbs free energy of activation ($\Delta G^{\ddagger}$, kJ mol^{-1}) and reaction ($\Delta_r G^0$, kJ mol^{-1}), thermal rate constant (k_T, M^{-1} s^{-1}), diffusion rate constant (k_D, M^{-1} s^{-1}), apparent rate constant (k_{app}, M^{-1} s^{-1}), apparent rate constant corrected by the molar fraction of Cur-III (k_{app}^{Mf}, M^{-1} s^{-1}), and branching ratio (Γ, %) of the reactions between the HOO• radical and the diketone tautomer of Cur-III in water and PEA.

Form	Position	$\Delta G^{\ddagger}$	$\Delta_r G^0$	k_T	k_D	k_{app}	k_{app}^{Mf}	Γ
WATER								
				Abstraction reaction				
	O22H	-1.8	86.1	2.61×10^{3}	2.38×10^{9}	2.61×10^{3}	1.13×10^{3}	0.06
	O23H	-1.8	85.1	3.36×10^{2}	2.38×10^{9}	3.36×10^{3}	1.46×10^{3}	0.07
				Addition reaction				
Neutral	C1	22.5	91.6	2.51×10^{-2}	1.97×10^{9}	2.51×10^{-2}	1.09×10^{-2}	0.00
(f_i = 43.33 %)	C2	8.4	83.2	5.43×10^{-1}	2.00×10^{9}	5.43×10^{-1}	2.35×10^{-1}	0.00
	C6	13.3	81.4	2.28×10^{0}	2.00×10^{9}	2.28×10^{0}	9.89×10^{-1}	0.00
	C7	21.9	90.6	3.77×10^{-2}	1.97×10^{9}	3.77×10^{-2}	1.63×10^{-2}	0.00
				Single electron transfer reaction				
		136.0	136.1	2.18×10^{-10}	8.42×10^{9}	2.18×10^{-10}	9.45×10^{-11}	0.00
				Abstraction reaction				
	O22H	-18.2	80.9	1.04×10^{4}	2.43×10^{9}	1.04×10^{4}	5.82×10^{3}	0.30
	O23H	-15.7	80.9	5.56×10^{3}	2.42×10^{9}	5.56×10^{3}	3.03×10^{3}	0.15
				Addition reaction				
	C1	11.9	88.2	9.43×10^{-2}	2.07×10^{9}	9.43×10^{-2}	5.13×10^{-2}	0.00
MonoAnion	C2	0.3	77.5	5.94×10^{0}	2.08×10^{9}	5.94×10^{0}	3.23×10^{0}	0.00
(f_i = 54.38 %)	C4	-7.0	62.5	1.87×10^{3}	1.96×10^{9}	1.87×10^{3}	1.02×10^{3}	0.05
	C6	11.6	78.7	3.39×10^{0}	2.05×10^{9}	3.39×10^{0}	1.82×10^{0}	0.00
	C7	17.9	83.6	5.49×10^{-1}	2.04×10^{9}	5.49×10^{-1}	2.99×10^{-1}	0.00
				Single electron transfer reaction				
		59.1	59.2	6.50×10^{3}	8.42×10^{9}	6.50×10^{3}	3.47×10^{3}	0.18
				Abstraction reaction				
	O22H	-15.1	83.9	9.29×10^{3}	2.41×10^{9}	9.29×10^{3}	2.10×10^{2}	0.01
				Addition reaction				
	C1	18.4	87.1	1.26×10^{-1}	2.03×10^{9}	1.26×10^{-1}	2.86×10^{-3}	0.00
DiAnion	C2	12.3	82.3	8.15×10^{-1}	2.04×10^{9}	8.15×10^{-1}	1.84×10^{-2}	0.00
(f_i = 2.26 %)	C4	-16.8	61.2	3.29×10^{3}	1.93×10^{9}	3.29×10^{3}	7.43×10^{1}	0.00
	C6	12.5	61.8	2.35×10^{3}	2.12×10^{9}	2.35×10^{3}	5.30×10^{1}	0.00
	C7	26.1	83.1	6.10×10^{-1}	2.03×10^{9}	6.10×10^{-1}	1.38×10^{-2}	0.00
				Single electron transfer reaction				
		15.5	35.8	8.13×10^{7}	8.44×10^{9}	8.06×10^{7}	1.82×10^{6}	92.71
				Addition reaction				
	C1	24.1	82.2	8.63×10^{-1}	2.08×10^{9}	8.63×10^{-1}	3.24×10^{-4}	0.00
	C2	4.7	57.2	1.53×10^{4}	2.22×10^{9}	1.53×10^{4}	5.74×10^{0}	0.00
TriAnion	C4	-4.6	55.1	3.81×10^{4}	1.95×10^{9}	3.81×10^{4}	1.43×10^{1}	0.00
(f_i = 0.04 %)	C6	9.4	59.9	5.07×10^{3}	2.18×10^{9}	5.07×10^{3}	1.90×10^{0}	0.00
	C7	24.1	82.9	6.62×10^{-1}	2.08×10^{9}	6.62×10^{-1}	2.48×10^{-4}	0.00
				Single electron transfer reaction				
		27.7	32.2	3.52×10^{8}	8.30×10^{9}	3.38×10^{8}	1.27×10^{5}	6.46
Total							1.96×10^{6}	100.00
PENTYL ETHANOATE								
				Abstraction reaction				
	O22H	4.8	84.0	1.01×10^{3}	2.63×10^{9}	1.01×10^{3}	1.01×10^{3}	90.13
	O23H	4.8	87.0	1.11×10^{2}	2.64×10^{9}	1.11×10^{2}	1.11×10^{2}	9.85
Neutral				Addition reaction				
(f_i = 100.00 %)	C1	23.3	98.9	1.25×10^{-3}	2.16×10^{9}	1.25×10^{-3}	1.25×10^{-3}	0.00
	C2	10.8	88.6	6.73×10^{-2}	2.18×10^{9}	6.73×10^{-2}	6.73×10^{-2}	0.01
	C6	25.4	88.0	8.53×10^{-2}	2.17×10^{9}	8.53×10^{-2}	8.53×10^{-2}	0.01
	C7	16.5	103.1	2.27×10^{-4}	2.16×10^{9}	2.27×10^{-4}	2.27×10^{-4}	0.00
Total							1.12×10^{3}	100.00

Table 5: The Gibbs free energy of activation ($\Delta G^{\ddagger}$, kJ mol^{-1}) and reaction ($\Delta_r G^0$, kJ mol^{-1}), thermal rate constant (k_T, M^{-1} s^{-1}), diffusion rate constant (k_D, M^{-1} s^{-1}), apparent rate constant (k_{app}, M^{-1} s^{-1}), apparent rate constant including the molar fraction of Cur-III (k_{app}^{Mf}, M^{-1} s^{-1}), and branching ratio (Γ, %) of the reactions between the HOO• radical and the keto-enol tautomer of Cur-III in water and PEA.

Form	Position	$\Delta G^{\ddagger}$	$\Delta_r G^0$	k_T	k_D	k_{app}	k_{app}^{Mf}	Γ
WATER								
				Abstraction reaction				
	O23H	-6.1	88.4	8.31×10^{2}	2.43×10^{9}	8.31×10^{2}	6.44×10^{2}	0.00
	O22H	-6.1	88.1	9.73×10^{2}	2.42×10^{9}	9.73×10^{2}	7.54×10^{2}	0.00
				Addition reaction				
Neutral	C1	14.0	89.4	5.84×10^{-2}	2.05×10^{9}	5.84×10^{-2}	4.53×10^{-2}	0.00
(f_i = 77.56 %)	C2	18.9	89.8	4.18×10^{-2}	2.05×10^{9}	4.18×10^{-2}	3.24×10^{-2}	0.00
	C4	11.8	87.4	9.74×10^{-2}	2.01×10^{9}	9.74×10^{-2}	7.55×10^{-2}	0.00
	C6	11.2	87.3	1.13×10^{-1}	2.05×10^{9}	1.13×10^{-1}	8.76×10^{-2}	0.00
	C7	16.5	97.2	2.59×10^{-3}	2.01×10^{9}	2.59×10^{-3}	2.01×10^{-2}	0.00
				Single electron transfer reaction				
		127.7	135.9	2.36×10^{-10}	8.28×10^{9}	2.36×10^{-10}	1.83×10^{-10}	0.00
				Abstraction reaction				
	O23H	-11.2	77.1	2.23×10^{4}	2.14×10^{9}	2.23×10^{4}	4.89×10^{3}	0.02
	O22H	-11.2	77.0	2.30×10^{4}	2.14×10^{9}	2.30×10^{4}	5.39×10^{3}	0.02
				Addition reaction				
MonoAnion	C1	15.6	90.4	3.52×10^{-2}	2.03×10^{9}	3.52×10^{-2}	7.73×10^{-3}	0.00
(f_i = 21.92 %)	C2	9.9	81.1	1.26×10^{0}	2.06×10^{9}	1.26×10^{0}	2.27×10^{-1}	0.00
	C4	-4.3	68.2	1.93×10^{2}	1.94×10^{9}	1.93×10^{2}	4.23×10^{1}	0.00
	C6	9.9	81.1	1.23×10^{0}	2.06×10^{9}	1.23×10^{0}	2.70×10^{-1}	0.00
	C7	17.4	91.1	3.04×10^{-2}	2.06×10^{9}	3.04×10^{-2}	6.66×10^{-3}	0.00
				Single electron transfer reaction				
		69.5	69.6	9.56×10^{1}	8.33×10^{9}	9.56×10^{1}	2.10×10^{1}	0.00
				Abstraction reaction				
	O23H	-14.4	81.1	3.41×10^{4}	2.04×10^{9}	3.41×10^{4}	1.73×10^{2}	0.00
				Addition reaction				
	C1	20.4	86.9	1.48×10^{-1}	2.03×10^{9}	1.48×10^{-1}	1.62×10^{-3}	0.00
DiAnion	C2	-8.1	55.6	4.95×10^{4}	2.25×10^{9}	4.95×10^{4}	5.42×10^{2}	0.00
(f_i = 0.51 %)	C4	-12.0	62.8	1.67×10^{3}	1.90×10^{9}	1.67×10^{3}	1.83×10^{1}	0.00
	C6	7.0	78.8	3.18×10^{0}	2.00×10^{9}	3.18×10^{0}	3.48×10^{-2}	0.00
	C7	14.8	88.3	8.30×10^{-2}	1.98×10^{9}	8.30×10^{-2}	9.08×10^{-4}	0.00
				Single electron transfer reaction				
		16.1	23.2	1.30×10^{10}	8.33×10^{9}	5.08×10^{9}	2.57×10^{7}	98.70
				Addition reaction				
	C1	21.8	76.6	8.16×10^{0}	2.05×10^{9}	8.16×10^{0}	8.20×10^{-4}	0.00
	C2	1.2	57.6	1.32×10^{4}	2.19×10^{9}	1.32×10^{4}	1.30×10^{0}	0.00
TriAnion	C4	-1.1	61.4	2.95×10^{3}	1.92×10^{9}	2.95×10^{3}	2.90×10^{-1}	0.00
(f_i = 0.01 %)	C6	1.5	60.8	3.58×10^{3}	2.15×10^{9}	3.58×10^{3}	3.51×10^{-1}	0.00
	C7	16.1	80.7	1.71×10^{0}	2.09×10^{9}	1.71×10^{0}	1.68×10^{-4}	0.00
				Single electron transfer reaction				
		11.8	25.3	5.52×10^{9}	8.40×10^{9}	3.33×10^{9}	3.27×10^{5}	1.26
Total							2.61×10^{7}	100.00
PENTYL ETHANOATE								
				Abstraction reaction				
	O22H	-3.7	85.7	4.61×10^{2}	2.68×10^{9}	4.61×10^{2}	4.61×10^{2}	56.52
	O23H	-0.8	86.4	3.55×10^{2}	2.68×10^{9}	3.55×10^{2}	3.55×10^{2}	43.48
				Addition reaction				
Neutral	C1	14.3	98.1	1.66×10^{-3}	2.23×10^{9}	1.66×10^{-3}	1.66×10^{-3}	0.00
(f_i = 100.00 %)	C2	27.3	95.3	4.54×10^{-3}	2.21×10^{9}	4.54×10^{-3}	4.54×10^{-3}	0.00
	C4	24.8	92.9	1.13×10^{-2}	2.20×10^{9}	1.13×10^{-2}	1.13×10^{-2}	0.00
	C6	21.4	93.6	9.07×10^{-3}	2.22×10^{9}	9.07×10^{-3}	9.07×10^{-3}	0.00
	C7	20.1	102.4	3.25×10^{-4}	2.21×10^{9}	3.25×10^{-4}	3.25×10^{-4}	0.00
Total							8.16×10^{2}	100.00

Tables 4 and **5** display the kinetic results for HOO scavenging reactions of the diketone and the keto-enol tautomers of Cur-III in water and PEA solvents. In water, the neutral diketone represents higher rate constants of FHT reaction than the neutral keto-enol compound (*i.e.*, $1.13 \times 10^3/1.46 \times 10^3$ $M^{-1}s^{-1}$ compared with $6.44 \times 10^2/7.54 \times 10^2$ $M^{-1}s^{-1}$ for FHT at O22H/O23H position). Conversely, the monoanion of diketone has lower FHT rate constants than the one of keto-enol at the same positions (*i.e.*, $5.82 \times 10^3/3.03 \times 10^3$ $M^{-1}s^{-1}$ compared with $4.89 \times 10^3/5.39 \times 10^3$ $M^{-1}s^{-1}$, respectively). It is noteworthy that the radical addition reaction at the C4 position of the monoanionic diketone represents an attractive rate constant being 1.02×10^3 $M^{-1}s^{-1}$, which contributes a significant ratio to its total rate constant. Finally, the dianion and trianion forms of the diketone and the keto-enol of Cur-III also react with the HOO radical essentially *via* SET reactions, as observed in the cases of Cur-I compounds. The SET rate constants of the dianion and trianion diketone compounds are equal to 1.82×10^6 and 1.27×10^5 $M^{-1}s^{-1}$, respectively, which are all lower than the ones of keto-enol (*i.e.*, 2.57×10^7 and 3.27×10^5 $M^{-1}s^{-1}$, respectively). In PEA solvent, the abstraction reaction also plays an essential role with the higher rate constants for Cur-I (*i.e.*, $1.01 \times 10^3/1.11 \times 10^2$ $M^{-1}s^{-1}$ for FHT at O22H/O23H, respectively) than Cur-III (*i.e.*, $4.61 \times 10^2/3.55 \times 10^2$ $M^{-1}s^{-1}$, respectively).

Table 6. The apparent diffusion-corrected rate constant (k_{app}, M^{-1} s^1), the molar fraction of tautomer form (M*f*, %), the total rate constant of each tautomer considering its molar fraction (k_{Mf}, M^{-1} s^{-1}), and its corresponding branching ratio (Γ, %) for the reactions between the $HOO^{\bullet}$ and Cur-I and Cur-III in water and PEA.

Tautomers	WATER				PEA			
	k_{app}	M*f*	k_{Mf}	Γ	k_{app}	M*f*	k_{Mf}	Γ
Curcumin-I								
Diketone	1.62×10^8	0.59	9.53×10^5	1.02	5.36×10^1	0.01	7.14×10^{-3}	0.02
Keto-enol	9.32×10^7	99.41	9.26×10^7	98.98	4.02×10^1	99.99	4.02×10^1	99.98
Overall			**9.36×10^7**	**100.00**			**4.02×10^1**	**100.00**
Curcumin-III								
Diketone	1.96×10^6	0.14	2.81×10^3	0.01	1.12×10^3	0.20	2.26×10^0	0.28
Keto-enol	2.61×10^7	99.86	2.60×10^7	99.99	8.15×10^2	99.80	8.14×10^2	99.72
Overall			**2.60×10^7**	**100.00**			**8.16×10^2**	**100.00**

Finally, **Table 6** resumes the total apparent rate constants of diketone and keto-enol tautomers and the overall rate constants of Cur-I and Cur-III considering the molar fraction of each tautomer in the aqueous phase and the PEA solvent.

Significantly, the keto-enol tautomer, serving as the predominant form of both Cur-I and Cur-III with molar fractions ranging from 99.40% to 99.90%, aligns closely with the findings of Galano *et al.* (2009) (Galano et al., 2009). This underscores the importance of the keto-enol tautomer in our understanding of the hydrogen transfer process. Notably, the total apparent rate constants (k_{Mf}) of keto-enol consistently surpass those of diketone. For instance, the (k_{Mf}) value of the keto-enol of Cur-I stands at 9.26×10^7

453 M^{-1} s^{-1}, accounting for 98.98%, a figure higher than the diketone's 9.53×10^5 M^{-1} s^{-1}, which represents
454 1.02%.

455 3.6. Is hydrogen abstraction a HAT or PCET process?

456 Regarding the hydrogen transfer process, several reaction mechanisms can occur in the biological
457 environment, which is complex and has different influencing factors. Concerted mechanisms (*i.e.*, hydrogen
458 atom transfer, HAT or proton-coupled electron transfer, PCET) or sequential ones (*i.e.*, sequential proton
459 loss-electron transfer, SPL-ET or sequential electron transfer-proton transfer, SET-PT) (Galano and Raúl
460 Alvarez-Idaboy, 2019; Mayer et al., 2002) may be involved in this transfer process. While the sequential
461 processes are distinguished via thermodynamic parameters based on the formation of different
462 intermediates, including radical anion or radical cation, respectively, the concerted ones are more difficult
463 to understand. Indeed, both HAT and PCET come from similar reactants and result in the same products;
464 thus, they cannot be thermodynamically differentiated. The difference between these two processes consists
465 in the way in which the charged particles (*i.e.*, electron and proton) are transported. In fact, both the electron
466 and proton are transferred *via* the same pathway in a whole package. At the same time, they are
467 independently shifted from different reactive sites of the donor molecule (DH) to the acceptor one (AH).
468 Thus, there have been some computational approaches that allow to distinguish the HAT from the PCET
469 process: (i) analysis of atomic charge and spin density of DH, AH, and transferred-H along the intrinsic
470 reaction coordinates (IRC) of the hydrogen transfer reaction, and (ii) analysis of singly occupied molecular
471 orbital (SOMO).

472 **Figure 8** displays the singly occupied molecular orbitals (SOMO) distributions for the transition states
473 (TSs) and the evolutions of spin densities and NPA atomic charges for hydrogen donor (DH), hydrogen (H)
474 and hydrogen acceptor (AH) along the intrinsic reaction coordinates (IRC) for the most preponderant
475 hydrogen abstraction processes at O22H and O23H positions (Abs-O22H and Abs-O23H) of Cur-I and
476 Cur-III compound in the aqueous phase.

477 The SOMO orbital distributions at the transition state of the H-transfer reaction have usually been evaluated
478 as a reliable indicator to distinguish the HAT or PCET process (Dao et al., 2017; Martínez et al., 2011).
479 Typically, for an HAT reaction, the SOMO of the TS has a high atomic orbital density distributed along the
480 H-transition vector, with the node plane located at the H species position. Conversely, for the PCET process,
481 SOMO of TS involves *p* orbitals that are orthogonal to the transition vector. Based on these indications, as
482 can be observed in Figure 8, both the most dominant TS for the abstraction reaction of the Cur-I, the *p*
483 orbital of the O species of H-donor (DH), and the one of H-acceptor (AH) form a bent angle being about

120 - 150°. A similar observation can be found for the abstraction reactions of Cur-III. This is the first signal indicating that the studied process may be a hydrogen transfer one.

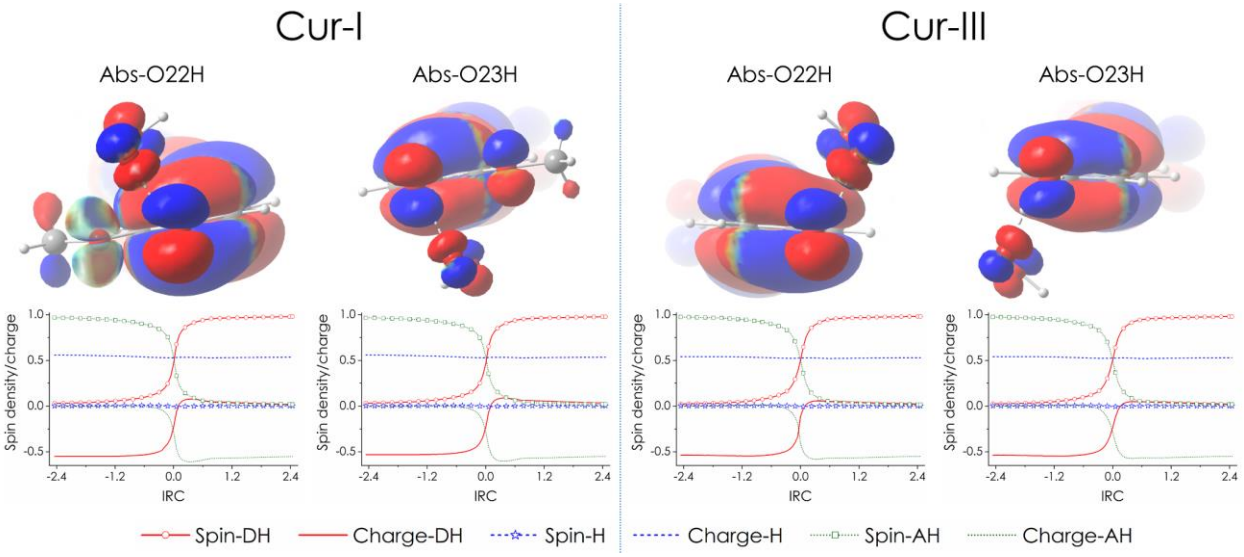

Figure 8: Evolutions of spin and NPA atomic charges for hydrogen donor (DH), hydrogen (H), and hydrogen acceptor (AH) along the intrinsic reaction coordinates (IRC) for the most preponderant hydrogen abstraction processes at O22H and O23H positions (Abs-O22H and Abs-O23H) of Cur-I and Cur-III compound in the aqueous phase. Singly occupied molecular orbitals (SOMO) for transition states (TSs) of each reaction computed with the iso-density value of 0.02 a.u. are also presented.

On the other hand, regarding the reaction at O22H of Cur I, the charge on the transferred H species remains around 0.53-0.55 e, which likely corresponds to a positively charged proton species. Meanwhile, the charge of H-donor (DH, the O species of Cur I) increases from about -0.55 *e* to a peak value of 0.07 *e* and then stabilizes at a value close to zero (*i.e.*, 0.02 *e*). One of the H-acceptors (AH) decreases from 0 to a minimum of -0.61 e and then slightly increases to about -0.55 e when the H is separated from the DH. Moreover, the spin density of transferred H is always zero along the IRC. At the same time, the one of DH increases strongly from 0.02 to 0.98, and the spin density of the AH reversely decreases from 0.97 to 0.02 when the HOO radical forms an H-O bond with the H species. The phenomenon occurring for the reaction at O23H of Cur I and both the ones at O22H and O23H of Cur III are similar.

Table 7: Natural electron configuration (NEC) for H species, H-donor (DH), and H-acceptor (AH, or HOO radical) analyzing at the transition state of the most dominant hydrogen transfer of Cur-I and Cur-III towards HOO radical in water.

CurI-O22H	H	$1S^{0}$
	O-DH	[core]$2S^{1.65}2p^{5.06}$
	O-AH	[core]$2S^{1.82}2p^{4.58}$
CurI-O23H	H	$1S^{0}$
	O-DH	[core]$2S^{0.83}2p^{2.47}$
	O-AH	[core]$2S^{0.91}2p^{2.12}$
CurIII-O22H	H	$1S^{0}$
	O-DH	[core]$2S^{0.83}2p^{2.42}$
	O-AH	[core]$2S^{0.90}2p^{2.24}$
CurIII-O23H	H	$1S^{0}$
	O-DH	[core]$2S^{0.83}2p^{2.42}$
	O-AH	[core]$2S^{0.90}2p^{2.20}$

Finally, natural electron configuration (NEC) analysis is investigated for H species, H-donor (DH), and H-acceptor (AH) species of the abstraction reaction transition states (**Figure 7**). All the H species involved possess a 1S0 electron configuration, which indicates the chemical structure of a proton. Meanwhile, both DH and AH display 2*p* orbital of the O species. All these observations confirm the chemical nature of the transferred H species being a proton, which is involved in a proton-coupled electron transfer (PCET) process.

4. Conclusions

The HOO radical scavenging reactions of two curcumin derivatives, namely curcumin I (Cur-I) and curcumin III (Cur-III), were evaluated in the water and pentyl ethanoate (PEA) solutions using Density functional theory DFT at the M06-2X/6-311++G(3df,3pd)//M06-2X/6-31+G(d,p) level of theory. Several intrinsic parameters (BDE, IP, PA), thermochemical parameters of the reaction ($\Delta_r G^0$ and $\Delta G^{\ddagger}$ at 298K), and the reaction kinetics were systematically calculated to predict three standard antioxidant processes, including HT, RAF, and SET. The contribution of the tautomerism phenomenon and the acid-base equilibrium in the solutions to the overall rate constants were characterized in detail by considering the reactions for both keto-enol and diketone forms, as well as the neutral, monoanionic, dianionic, and trianionic forms of two curcumin derivatives. The obtained conclusions are multiple:

(i) Cur-I and Cur-III mainly exist in the keto-enol tautomer form rather than the diketone one, with a molar fraction of the keto-enol of 99.4 and 99.9 %, respectively. At the same time, both the curcumins are predominantly present in the neutral and monoanionic forms with molar fraction from 98 to 99%. In comparison, the dianionic and trianionic ones possess only 1.0-2.0% in the water.

(ii) In water, the reactions of the neutral and monoanionic forms occur mainly *via* the HT processes at the phenolic hydroxyl groups (*i.e.,* O22H and O23H) rather than the RAF and SET ones. Conversely, the SET processes are the most dominant for the dianionic and trianionic forms. Among them, the SET reactions of the dianionic form play crucial roles with branching ratio values up to 98.70 % / 92.71 % and 97.60 % / 98.35 % for the keto-enol / diketone forms of the Cur-I and Cur-III, respectively. It is interestingly noted that the dianionic and trianionic forms contribute the most significant parts in the reaction of both the curcumin derivatives, although they have small molar fractions.

(iii) In PEA, the HT reactions at the phenolic HO groups (O22H and O23H) are, as expected, the most predominant reactions (branching ratios of about 100%) of both the tautomers of Cur-I and Cur-III derivatives.

(iv) Since the keto-enol tautomer consists of the most dominant existing form compared to the diketone one for both Cur-I and Cur-III, the keto-enol forms contribute the most significant fraction in the overall reaction rates, with branching ratio values of about 100.00 %. The rate constants of the keto-enol form are 9.26×10^7 and 2.60×10^7 M^{-1} s^{-1} in water for Cur-I and Cur-II, respectively. At the same time, the values in the PEA solution are 4.02×10^1 and 8.14×10^2 M^{-1} s^{-1}, respectively.

(v) Overall rate constants of the reactions in water are 9.36×10^7 and 2.60×10^7 M^{-1} s^{-1}, for Cur-I and Cur-III, respectively. Meanwhile, the ones in PEA are significantly less important, 4.02×10^1 and 8.06×10^2 M^{-1} s^{-1}, respectively. In possessing two peroxy substituents in the phenolic rings, Cur-I represents a higher rate constant than Cur-III in water because of the electron-donating effects of the CH_3O groups in the SET reaction of the dianionic form of Cur-I. At the same time, the Cur-III has higher rate constants than the Cur-I in the PEA solution.

(vi) The analyses of SOMO orbitals, atomic charges, spin densities along the IRC, and natural electron configuration NEC show that all the hydrogen transfer processes occur *via* the proton-coupled electron transfer (PCET) mechanism.

The actual computational study may contribute a systematic point of view on the radical scavenging activities of the curcumin derivatives, as well as the influence of various critical factors like the acid-base

equilibrium and the tautomerism on reaction rates. It also has further implications for curcumin derivatives in various medicinal applications.

Acknowledgments

This work was supported by the Vietnam Academy of Science and Technology (Grant QTPL01.02/22-23). This work used the Extreme Science and Engineering Discovery Environment (XSEDE), which is supported by National Science Foundation grant number OCI-1053575. SEAGrid (http:www.seagrid.org) (Milfeld, 2005; Dooley et al., 2006; Shen et al., 2014; Pamidighantam et al., 2016) is acknowledged for computational resources and services for the selected results used in this publication.

References

Alecu, I.M., Zheng, J., Zhao, Y., Truhlar, D.G., 2010. Computational Thermochemistry: Scale Factor Databases and Scale Factors for Vibrational Frequencies Obtained from Electronic Model Chemistries. J. Chem. Theory Comput. 6, 2872–2887. https://doi.org/10.1021/ct100326h

Alisi, I.O., Uzairu, A., Abechi, S.E., 2020. Molecular design of curcumin analogues with potent antioxidant properties and thermodynamic evaluation of their mechanism of free radical scavenge. Bull. Natl. Res. Cent. 44, 137. https://doi.org/10.1186/s42269-020-00391-z

Anjomshoa, S., Namazian, M., Noorbala, M.R., 2017. Is curcumin a good scavenger of reactive oxygen species? A computational investigation. Theor. Chem. Acc. 136, 103. https://doi.org/10.1007/s00214-017-2128-5

Anjomshoa, S., Namazian, M., Noorbala, M.R., 2016. The Effect of Solvent on Tautomerism, Acidity and Radical Stability of Curcumin and Its Derivatives Based on Thermodynamic Quantities. J. Solut. Chem. 45, 1021–1030. https://doi.org/10.1007/s10953-016-0481-y

Arun, N., Nalini, N., 2002. Efficacy of turmeric on blood sugar and polyol pathway in diabetic albino rats. Plant Foods Hum. Nutr. 57, 41–52. https://doi.org/10.1023/A:1013106527829

Barclay, L.R.C., Vinqvist, M.R., Mukai, K., Goto, H., Hashimoto, Y., Tokunaga, A., Uno, H., 2000. On the Antioxidant Mechanism of Curcumin: Classical Methods Are Needed To Determine Antioxidant Mechanism and Activity. Org. Lett. 2, 2841–2843. https://doi.org/10.1021/ol000173t

Boulmokh, Y., Belguidoum, K., Meddour, F., Amira-Guebailia, H., 2024. Enhanced antioxidant properties of novel curcumin derivatives: a comprehensive DFT computational study. Struct. Chem. 35, 825–839. https://doi.org/10.1007/s11224-023-02237-6

Cannizzo, E.S., Clement, C.C., Sahu, R., Follo, C., Santambrogio, L., 2011. Oxidative stress, inflamm-aging and immunosenescence. J. Proteomics 74, 2313–2323. https://doi.org/10.1016/j.jprot.2011.06.005

590 Chen, W., Zheng, J., Bao, J.L., Truhlar, D.G., Xu, X., 2023. MSTor 2023: A new version of the computer code
591 for multistructural torsional anharmonicity, now with automatic torsional identification using redundant
592 internal coordinates. Comput. Phys. Commun. 288, 108740. https://doi.org/10.1016/j.cpc.2023.108740

593 Collins, F.C., Kimball, G.E., 1949. Diffusion-controlled reaction rates. J. Colloid Sci. 4, 425–437.
594 https://doi.org/10.1016/0095-8522(49)90023-9

595 Dao, D.Q., Ngo, T.C., Thong, N.M., Nam, P.C., 2017. Is Vitamin A an Antioxidant or a Pro-oxidant? J. Phys.
596 Chem. B 121, 9348–9357. https://doi.org/10.1021/acs.jpcb.7b07065

597 Dao, D.Q., Taamalli, S., Louis, F., Kdouh, D., Srour, Z., Ngo, T.C., Truong, D.H., Fèvre-Nollet, V., Ribaucour,
598 M., El Bakali, A., Černušák, I., 2023. Hydroxyl radical-initiated decomposition of metazachlor herbicide in
599 the gaseous and aqueous phases: Mechanism, kinetics, and toxicity evaluation. Chemosphere 312,
600 137234. https://doi.org/10.1016/j.chemosphere.2022.137234

601 Duvoix, A., Blasius, R., Delhalle, S., Schnekenburger, M., Morceau, F., Henry, E., Dicato, M., Diederich, M.,
602 2005. Chemopreventive and therapeutic effects of curcumin. Cancer Lett. 223, 181–190.
603 https://doi.org/10.1016/j.canlet.2004.09.041

604 Dykstra, C.E. (Ed.), 2005. Theory and applications of computational chemistry: the first forty years, 1st ed.
605 ed. Elsevier, Amsterdam ; Boston.

606 Feller, D., 1996. The role of databases in support of computational chemistry calculations. J. Comput.
607 Chem. 17, 1571–1586. https://doi.org/10.1002/(SICI)1096-987X(199610)17:13<1571::AID-
608 JCC9>3.0.CO;2-P

609 Franceschi, C., Bonafè, M., Valensin, S., Olivieri, F., De Luca, M., Ottaviani, E., De Benedictis, G., 2000.
610 Inflamm-aging: An Evolutionary Perspective on Immunosenescence. Ann. N. Y. Acad. Sci. 908, 244–254.
611 https://doi.org/10.1111/j.1749-6632.2000.tb06651.x

612 Frisch, M.J., Trucks, G.W., Schlegel, H.B., Scuseria, G.E., Robb, M.A., Cheeseman, J.R., Scalmani, G., Barone,
613 V., Petersson, G.A., Nakatsuji, H., Li, X., Caricato, M., Marenich, A.V., Bloino, J., Janesko, B.G., Gomperts,
614 R., Mennucci, B., Hratchian, H.P., Ortiz, J.V., Izmaylov, A.F., Sonnenberg, J.L., Williams, Ding, F., Lipparini,
615 F., Egidi, F., Goings, J., Peng, B., Petrone, A., Henderson, T., Ranasinghe, D., Zakrzewski, V.G., Gao, J., Rega,
616 N., Zheng, G., Liang, W., Hada, M., Ehara, M., Toyota, K., Fukuda, R., Hasegawa, J., Ishida, M., Nakajima,
617 T., Honda, Y., Kitao, O., Nakai, H., Vreven, T., Throssell, K., Montgomery Jr., J.A., Peralta, J.E., Ogliaro, F.,
618 Bearpark, M.J., Heyd, J.J., Brothers, E.N., Kudin, K.N., Staroverov, V.N., Keith, T.A., Kobayashi, R., Normand,
619 J., Raghavachari, K., Rendell, A.P., Burant, J.C., Iyengar, S.S., Tomasi, J., Cossi, M., Millam, J.M., Klene, M.,
620 Adamo, C., Cammi, R., Ochterski, J.W., Martin, R.L., Morokuma, K., Farkas, O., Foresman, J.B., Fox, D.J.,
621 2016. Gaussian 16 Rev. C.01.

622 Galano, A., Álvarez-Diduk, R., Ramírez-Silva, M.T., Alarcón-Ángeles, G., Rojas-Hernández, A., 2009. Role of
623 the reacting free radicals on the antioxidant mechanism of curcumin. Chem. Phys. 363, 13–23.
624 https://doi.org/10.1016/j.chemphys.2009.07.003

625 Galano, A., Raúl Alvarez-Idaboy, J., 2019. Computational strategies for predicting free radical scavengers'
626 protection against oxidative stress: Where are we and what might follow? Int. J. Quantum Chem. 119,
627 e25665. https://doi.org/10.1002/qua.25665

Gruver, A., Hudson, L., Sempowski, G., 2007. Immunosenescence of ageing. J. Pathol. 211, 144–156. https://doi.org/10.1002/path.2104

Gupta, S.C., Patchva, S., Aggarwal, B.B., 2013. Therapeutic Roles of Curcumin: Lessons Learned from Clinical Trials. AAPS J. 15, 195–218. https://doi.org/10.1208/s12248-012-9432-8

Hazarika, R., Kalita, B., 2021. Elucidating the therapeutic activity of selective curcumin analogues: DFT-based reactivity analysis. Struct. Chem. 32, 1701–1715. https://doi.org/10.1007/s11224-021-01745-7

Hratchian, H.P., Schlegel, H.B., 2005. Using Hessian Updating To Increase the Efficiency of a Hessian Based Predictor-Corrector Reaction Path Following Method. J. Chem. Theory Comput. 1, 61–69. https://doi.org/10.1021/ct0499783

Hratchian, H.P., Schlegel, H.B., 2004. Accurate reaction paths using a Hessian based predictor–corrector integrator. J. Chem. Phys. 120, 9918–9924. https://doi.org/10.1063/1.1724823

K. Al Rawas, H., Al Mawla, R., Pham, T.Y.N., Truong, D.H., Nguyen, T.L.A., Taamalli, S., Ribaucour, M., El Bakali, A., Černušák, I., Dao, D.Q., Louis, F., 2023. New insight into environmental oxidation of phosmet insecticide initiated by $HO^{\cdot}$ radicals in gas and water – a theoretical study. Environ. Sci. Process. Impacts 10.1039.D3EM00325F. https://doi.org/10.1039/D3EM00325F

Kumaraswamy, P., Sethuraman, S., Krishnan, U.M., 2013. Mechanistic Insights of Curcumin Interactions with the Core-Recognition Motif of β-Amyloid Peptide. J. Agric. Food Chem. 61, 3278–3285. https://doi.org/10.1021/jf4000709

Lao, L., Cui, J.-H., Gerla, M., Maggiorini, D., 2006. A Comparative Study of Multicast Protocols: Top, Bottom, or In the Middle?, in: Proceedings IEEE INFOCOM 2006. 25TH IEEE International Conference on Computer Communications. Presented at the Proceedings IEEE INFOCOM 2006. 25TH IEEE International Conference on Computer Communications, IEEE, Barcelona, Spain, pp. 1–6. https://doi.org/10.1109/INFOCOM.2006.344

Lim, G.P., Chu, T., Yang, F., Beech, W., Frautschy, S.A., Cole, G.M., 2001. The Curry Spice Curcumin Reduces Oxidative Damage and Amyloid Pathology in an Alzheimer Transgenic Mouse. J. Neurosci. 21, 8370–8377. https://doi.org/10.1523/JNEUROSCI.21-21-08370.2001

Lovell, M.A., Robertson, J.D., Teesdale, W.J., Campbell, J.L., Markesbery, W.R., 1998. Copper, iron and zinc in Alzheimer's disease senile plaques. J. Neurol. Sci. 158, 47–52. https://doi.org/10.1016/S0022-510X(98)00092-6

Manzanilla, B., Robles, J., 2022. Antiradical properties of curcumin, caffeic acid phenethyl ester, and chicoric acid: a DFT study. J. Mol. Model. 28, 68. https://doi.org/10.1007/s00894-022-05056-4

Marcus, R.A., 1957a. On the Theory of Oxidation-Reduction Reactions Involving Electron Transfer. III. Applications to Data on the Rates of Organic Redox Reactions. J. Chem. Phys. 26, 872–877. https://doi.org/10.1063/1.1743424

Marcus, R.A., 1957b. On the Theory of Oxidation-Reduction Reactions Involving Electron Transfer. II. Applications to Data on the Rates of Isotopic Exchange Reactions. J. Chem. Phys. 26, 867–871. https://doi.org/10.1063/1.1743423

Marcus, R.A., 1956. On the Theory of Oxidation-Reduction Reactions Involving Electron Transfer. I. J. Chem. Phys. 24, 966–978. https://doi.org/10.1063/1.1742723

Marenich, A.V., Cramer, C.J., Truhlar, D.G., 2009. Universal Solvation Model Based on Solute Electron Density and on a Continuum Model of the Solvent Defined by the Bulk Dielectric Constant and Atomic Surface Tensions. J. Phys. Chem. B 113, 6378–6396. https://doi.org/10.1021/jp810292n

Martínez, A., Galano, A., Vargas, R., 2011. Free Radical Scavenger Properties of α-Mangostin: Thermodynamics and Kinetics of HAT and RAF Mechanisms. J. Phys. Chem. B 115, 12591–12598. https://doi.org/10.1021/jp205496u

Masuda, T., Maekawa, T., Hidaka, K., Bando, H., Takeda, Y., Yamaguchi, H., 2001. Chemical Studies on Antioxidant Mechanism of Curcumin: Analysis of Oxidative Coupling Products from Curcumin and Linoleate. J. Agric. Food Chem. 49, 2539–2547. https://doi.org/10.1021/jf001442x

Mayer, J.M., Hrovat, D.A., Thomas, J.L., Borden, W.T., 2002. Proton-Coupled Electron Transfer versus Hydrogen Atom Transfer in Benzyl/Toluene, Methoxyl/Methanol, and Phenoxyl/Phenol Self-Exchange Reactions. J. Am. Chem. Soc. 124, 11142–11147. https://doi.org/10.1021/ja012732c

M.C. Recio, I. Andujar, J.L. Rios, 2012. Anti-Inflammatory Agents from Plants: Progress and Potential. Curr. Med. Chem. 19, 2088–2103. https://doi.org/10.2174/092986712800229069

Menon, V.P., Sudheer, A.R., 2007. Antioxidant and anti-inflammatory properties of Curcumin, in: Aggarwal, B.B., Surh, Y.-J., Shishodia, S. (Eds.), The Molecular Targets and Therapeutic Uses of Curcumin in Health and Disease, ADVANCES IN EXPERIMENTAL MEDICINE AND BIOLOGY. Springer US, Boston, MA, pp. 105–125. https://doi.org/10.1007/978-0-387-46401-5_3

Miyoshi, A., 2022. GPOP software, rev. 2022.01.20m1, available from the author. See http://akrmys.com/gpop/.

Moore, T.L., Bowley, B.G.E., Shultz, P.L., Calderazzo, S.M., Shobin, E.J., Uprety, A.R., Rosene, D.L., Moss, M.B., 2018. Oral curcumin supplementation improves fine motor function in the middle-aged rhesus monkey. Somatosens. Mot. Res. 35, 1–10. https://doi.org/10.1080/08990220.2018.1432481

Motterlini, R., Foresti, R., Bassi, R., Green, C.J., 2000. Curcumin, an antioxidant and anti-inflammatory agent, induces heme oxygenase-1 and protects endothelial cells against oxidative stress. Free Radic. Biol. Med. 28, 1303–1312. https://doi.org/10.1016/S0891-5849(00)00294-X

Mukhopadhyay, A., Basu, N., Ghatak, N., Gujral, P.K., 1982. Anti-inflammatory and irritant activities of curcumin analogues in rats. Agents Actions 12, 508–515. https://doi.org/10.1007/BF01965935

Mukhopadhyay, A., Bueso-Ramos, C., Chatterjee, D., Pantazis, P., Aggarwal, B.B., 2001. Curcumin downregulates cell survival mechanisms in human prostate cancer cell lines. Oncogene 20, 7597–7609. https://doi.org/10.1038/sj.onc.1204997

Negi, P.S., Jayaprakasha, G.K., Jagan Mohan Rao, L., Sakariah, K.K., 1999. Antibacterial Activity of Turmeric Oil: A Byproduct from Curcumin Manufacture. J. Agric. Food Chem. 47, 4297–4300. https://doi.org/10.1021/jf990308d

Ngo, T.C., Taamalli, S., Srour, Z., Fèvre-Nollet, V., El Bakali, A., Louis, F., Černušák, I., Dao, D.Q., 2023. Theoretical insights into the oxidation of quinmerac herbicide initiated by HO• radical in aqueous media: Mechanism, kinetics, and ecotoxicity. J. Environ. Chem. Eng. 11, 109941. https://doi.org/10.1016/j.jece.2023.109941

Panahi, Y., Hosseini, M.S., Khalili, N., Naimi, E., Simental-Mendía, L.E., Majeed, M., Sahebkar, A., 2016. Effects of curcumin on serum cytokine concentrations in subjects with metabolic syndrome: A post-hoc analysis of a randomized controlled trial. Biomed. Pharmacother. 82, 578–582. https://doi.org/10.1016/j.biopha.2016.05.037

Park, S.-Y., Kim, H.-S., Cho, E.-K., Kwon, B.-Y., Phark, S., Hwang, K.-W., Sul, D., 2008. Curcumin protected PC12 cells against beta-amyloid-induced toxicity through the inhibition of oxidative damage and tau hyperphosphorylation. Food Chem. Toxicol. 46, 2881–2887. https://doi.org/10.1016/j.fct.2008.05.030

Perrone, D., Ardito, F., Giannatempo, G., Dioguardi, M., Troiano, G., Lo Russo, L., De Lillo, A., Laino, L., Lo Muzio, L., 2015. Biological and therapeutic activities, and anticancer properties of curcumin. Exp. Ther. Med. 10, 1615–1623. https://doi.org/10.3892/etm.2015.2749

Pritchard, B.P., Altarawy, D., Didier, B., Gibson, T.D., Windus, T.L., 2019. New Basis Set Exchange: An Open, Up-to-Date Resource for the Molecular Sciences Community. J. Chem. Inf. Model. 59, 4814–4820. https://doi.org/10.1021/acs.jcim.9b00725

Priyadarsini, K.I., Maity, D.K., Naik, G.H., Kumar, M.S., Unnikrishnan, M.K., Satav, J.G., Mohan, H., 2003. Role of phenolic O-H and methylene hydrogen on the free radical reactions and antioxidant activity of curcumin. Free Radic. Biol. Med. 35, 475–484. https://doi.org/10.1016/S0891-5849(03)00325-3

Ramirez-Boscá, A., Soler, A., Carrión Gutierrez, M.A., Laborda Alvarez, J., Quintanilla Almagro, E., 1995. Antioxidant Curcuma extracts decrease the blood lipid peroxide levels of human subjects. AGE 18, 167–169. https://doi.org/10.1007/BF02432631

Rao, P.P.N., Mohamed, T., Teckwani, K., Tin, G., 2015. Curcumin Binding to Beta Amyloid: A Computational Study. Chem. Biol. Drug Des. 86, 813–820. https://doi.org/10.1111/cbdd.12552

Rebollar-Zepeda, A.M., Campos-Hernández, T., Ramírez-Silva, M.T., Rojas-Hernández, A., Galano, A., 2011. Searching for Computational Strategies to Accurately Predict p K_a s of Large Phenolic Derivatives. J. Chem. Theory Comput. 7, 2528–2538. https://doi.org/10.1021/ct2001864

Sadatsharifi, M., Purgel, M., 2021. Radical scavenger competition of alizarin and curcumin: a mechanistic DFT study on antioxidant activity. J. Mol. Model. 27, 166. https://doi.org/10.1007/s00894-021-04778-1

Santos-Parker, J.R., Lubieniecki, K.L., Rossman, M.J., Van Ark, H.J., Bassett, C.J., Strahler, T.R., Chonchol, M.B., Justice, J.N., Seals, D.R., 2018. Curcumin supplementation and motor-cognitive function in healthy middle-aged and older adults. Nutr. Healthy Aging 4, 323–333. https://doi.org/10.3233/NHA-170029

Schuchardt, K.L., Didier, B.T., Elsethagen, T., Sun, L., Gurumoorthi, V., Chase, J., Li, J., Windus, T.L., 2007. Basis Set Exchange: A Community Database for Computational Sciences. J. Chem. Inf. Model. 47, 1045–1052. https://doi.org/10.1021/ci600510j

Singh, R., 2017. Combinatorial effect of curcumin with docetaxel modulates apoptotic and cell survival molecules in prostate cancer. Front. Biosci. 9, 235–245. https://doi.org/10.2741/e798

Singleton, D.L., Cvetanovic, R.J., 1976. Temperature Dependence of the Reactions of Oxygen Atoms with Olefins. J. Am. Chem. Soc.

Smoluchowski, M. v., 1918. Versuch einer mathematischen Theorie der Koagulationskinetik kolloider Lösungen. Zeitschrift für Physikalische Chemie 92U, 129–168. https://doi.org/10.1515/zpch-1918-9209

Toda, S., Miyase, T., Arichi, H., Tanizawa, H., Takino, Y., 1985. Natural antioxidants. III. Antioxidative components isolated from rhizome of Curcuma longa L. Chem. Pharm. Bull. (Tokyo) 33, 1725–1728. https://doi.org/10.1248/cpb.33.1725

Tomeh, M.A., Hadianamrei, R., Zhao, X., 2019. A Review of Curcumin and Its Derivatives as Anticancer Agents. Int. J. Mol. Sci. 20, 1033. https://doi.org/10.3390/ijms20051033

Vera-de La Garza, C.G., Martinez, R.J., Belmont-Bernal, F., 2023. Electronic structure of curcuminoids with potential medicinal applications: a theoretical insight. Struct. Chem. 34, 1427–1438. https://doi.org/10.1007/s11224-022-02080-1

Wilken, R., Veena, M.S., Wang, M.B., Srivatsan, E.S., 2011. Curcumin: A review of anti-cancer properties and therapeutic activity in head and neck squamous cell carcinoma. Mol. Cancer 10, 12. https://doi.org/10.1186/1476-4598-10-12

Yang, F., Lim, G.P., Begum, A.N., Ubeda, O.J., Simmons, M.R., Ambegaokar, S.S., Chen, P.P., Kayed, R., Glabe, C.G., Frautschy, S.A., Cole, G.M., 2005. Curcumin Inhibits Formation of Amyloid β Oligomers and Fibrils, Binds Plaques, and Reduces Amyloid in Vivo. J. Biol. Chem. 280, 5892–5901. https://doi.org/10.1074/jbc.M404751200

Zhao, L.N., Chiu, S.-W., Benoit, J., Chew, L.Y., Mu, Y., 2012. The Effect of Curcumin on the Stability of Aβ Dimers. J. Phys. Chem. B 116, 7428–7435. https://doi.org/10.1021/jp3034209

Zhao, Y., Truhlar, D.G., 2008. The M06 suite of density functionals for main group thermochemistry, thermochemical kinetics, noncovalent interactions, excited states, and transition elements: two new functionals and systematic testing of four M06-class functionals and 12 other functionals. Theor. Chem. Acc. 120, 215–241. https://doi.org/10.1007/s00214-007-0310-x